Scour variability across offshore wind farms (OWFs): Identifying 1 site-specific scour drivers as a step towards assessing potential 2 impacts on the marine environment 3 4 Karen Garcia1*, Christian Jordan1, Gregor Melling3, Alexander Schendel1,2, Mario Welzel1, Torsten 5 $Schlurmann^{1,2}$ 6 7 ¹Leibniz University Hannover, Ludwig-Franzius-Institute for Hydraulic, Estuarine and Coastal Engineering, 8 Nienburger Str. 4, 30167 Hannover, Germany. Email: schendel@lufi.uni-hannover.de, jordan@lufi.uni-9 hannover.de, welzel@lufi.uni-hannover.de, schlurmann@lufi.uni-hannover.de 10 ²Coastal Research Centre, Leibniz University Hannover & Technical University Braunschweig, Merkurstraße 11 11, 30419 Hannover, Germany. ³ Federal Waterways Engineering and Research Institute (BAW), Wedeler Landstraße 157, 22559 Hamburg, 12 13 Germany. Email: gregor.melling@baw.de 14 *Corresponding author: garcia@lufi.uni-hannover.de Abstract. The development of offshore wind farms (OWFs) is critical to meeting renewable energy targets, but 15 16 predicting scour around offshore wind energy structures (OWES) and the associated potential impacts on marine 17 ecosystems remains a challenge. Using high-resolution bathymetry data, this study analyses field-measured scour depths at 460 monopiles at nine British OWFs. The analysis reveals a large spatial variability of relative scour 18 depth (S/D) between OWF sites, but also within individual wind farms. Principal Ceomponent A Analysis (PCA) 19 is used to identify significant drivers of this variability. When the entire data set is considered, results indicate that 20 the relative water depth (h/D), the relative median grain size $(\frac{D}{d_{50}}/\frac{1}{d_{50}})$, Keulegan-Carpenter number (KC_{99}) , 21 and the sediment mobility parameter MOB $(\theta_{99}/\theta_{cr})$ are the most important influencing factors for the variability 22 of relative scour depth. Other parameters investigated, such as pile Reynolds number (Re_{99}), flow intensity $(U/U_{rr})_{99}$, and Froude number (Fr_{99}) , were found to have a less clear influence. Further sediment-specific analysis shows that relative water depth (h/D) is a particularly relevant driver of scour at sites with fine $(63 \le d_{50} < -200)$ 25 26 μm) and medium sands (200 $\leq d_{50} <$ 630 μm), with larger relative scour depth occurring in shallower relative 27 water depth. Findings from this study provide new insights into scour behaviour across a range of spatial and environmental 28 29 scales and lay a foundation for the transferability of scour prediction frameworks to new OWFs sites. In the future, 30 findings and datasets from this study are suggested to be used to estimate scour-induced sediment transport and thereby to provide a step towards the assessment of potential impacts of OWFs expansion scenarios in the marine 31 32 environment. By addressing the broader implications for regional sediment dynamics, this research contributes to 33 the sustainable development of offshore wind energy. 34 Keywords: Offshore wind farms (OWFs), relative scour depth, monopile, sediment transport, Pprincipal 36 Ceomponent aAnalysis (PCA).

1 Introduction & Motivation

39

38

40 The expansion of renewable energy is crucial for a sustainable and independent energy supply. In order to meet the European Union's targets for expanding offshore wind energy (EU, 2020), it is necessary to develop areas with 41 previously unveiled metoceanic and geophysical conditions. To this end, existing knowledge gaps about the 42 43 interaction of individual offshore wind energy structures (OWES) or entire offshore wind farms (OWFs) with the 44 marine environment must be closed. In general, the disturbance of the flow by an offshore structure causes scour, 45 which might not only affect the structure's stability (Saathoff et al., 2024), but the mobilized sediment may also contribute to the overall regional sediment transport (Vanhellemont et al., 2014; Baeye and Fettweis, 2015; Rivier 46 et al., 2016) with potential impacts on the marine environment. 47

The scour process itself, is a multivariate process, which is dependent on a combination of complex hydrodynamic

and geotechnical drivers. Early studies focused on the understanding of the scour process around a pile under

48 49

50

simplified isolated hydraulic conditions, such as steady flow (e.g., Sheppard et al., 2004; Zhao et al., 2012; Sarkar 51 et al., 2014; Baykal et al., 2015), -unsteady and bidirectional tidal currents (e.g., Escarameia and May_1999; 52 McGovern et al., 2014; Yao et al., 2016; Schendel et al., 2018) and waves (e.g., Sumer et al., 1992b; Carreiras et 53 al., 2001;-Stahlmann et al., 2013). With the availability of more sophisticated experimental facilities and numerical 54 55 models, research is increasingly shifting toward more complex hydrodynamic loads consisting of a combination 56 of waves and currents, as in the studies of Sumer and Fredsøe (2001), Qi and Gao (2014), Schendel et al. (2020), Lyu et al. (2021), and Du et al. (2022) and also towards studies addressing complex offshore structures (Welzel, 57 58 2021; Welzel et -al., 2024; Sarmiento et al., 2024; Chen et al., 2025). 59 Despite those advances in scour research, uncertainties remain in current scour prediction methods (Chen et al., 2024). Matutano et al. (2013) demonstrated the challenges of applying empirical formulas for maximum scour 60 depth by comparing different methods with data from ten European OWFs, revealing overpredictions in all but 61 two cases. The comparison highlights the fundamental challenge of accounting for complex marine flow conditions, characteriszed by the combined effect of multiple influencing factors, such as flow velocity, sediment 63 coarseness, and wave-current interactions, in the prediction of scour processes using existing models (Gazi et al., 64 2020; Harris et al., 2023). Compared to laboratory experiments focusing on scour processes, rather few studies are 65 based on in-situ data, thatdata, which represent the actual scour development under complex flow conditions. These studies assessed the scour at individual structures, such as monopiles (Walker, 1995; Noormets et al., 2003; 67 Harris et al., 2004; Rudolph et al., 2004; Louwersheimer et al., 2009), and jackets (Bolle et al., 2012; Baelus et al., 68 2018), or dealt with larger datasets from entire offshore wind projects (DECC 2008; COWRIE 2010; Whitehouse 69 et al., 2010; Whitehouse et al., 2011; Melling (2015)), covering both spatial and temporal evolution of scour under different hydrodynamic regimes and seabed types across the North Sea and British continental shelf. In general, 71 72 the amount and variety of field data collected has increased with the gradual installation of OWES. Focusing 73 specifically on the correlation between scour and on-site conditions, Melling (2015) analysed the relationships 74 between the variations of scour hole dimension within OWFs and both sedimentological and hydrodynamic parameters of 281 OWES in the Outer Thames estuary. Melling's (2015) study, although only covering three 75 OWFs, represents one of the most comprehensive investigations of field-related scour to date, with the highest number of structures examined so far. By comparing field data with physical modelling experiments and literature, the study provided valuable insights into the range of observed scour and its controlling structural, hydrodynamic, and sedimentological parameters.

In addition to local scour at individual structures, the cumulative effect of multiple structures in an OWFs can alter

80

81 ocean dynamics (Christiansen et al., 2022), mixing (Schultze et al., 2020), and sediment mobility, resulting in 82 changes to suspended sediment concentrations and wave-induced turbidity plumes (Vanhellemont & Ruddick, 2014). This can also lead to dynamic interactions with migrating seabed features, such as sand waves (Matthieu & 83 Raaijmakers, 2012). Increased velocities and turbulence induced by OWFs hasve also the potential to affect the 84 85 marine environment, potentially leading to global erosion around the structures as well as habitat loss or gain for 86 benthic flora and fauna (Shields et al., 2011; Wilson and Elliott, 2009; Welzel et al., 2019). Concerns over the 87 potential impacts of OWF installations on local ecosystems further include collision risks, noise pollution, electromagnetic fields, and the introduction of invasive species (Lloret et al., 2022; Bailey et al., 2014; Teilmann 88 89 and Carstensen, 2012; Watson et al., 2024). As the size and scale of OWF increases, the risk of significant 90 cumulative effects arising is also expected to increase (Brignon et al., 2022; Gușatu et al., 2021). The drivers and 91 interdependencies of these large-scale processes are not yet well understood, and the precise impact of scour-92 induced sediment transport on the marine environment remains uncertain, highlighting the need for 93 interdisciplinary research utilizing field data. 94 In order to gain a better understanding of the geophysical changes following the installation of OWFs and potential impacts on the marine environment arising from it, this study analyses the scour development at OWES as a first 95 96 step. This study builds its analysis on field data, including high-resolution bathymetry scans from British OWFs, which have recently been made publicly available. This provides an opportunity to extend the understanding of 97 98 scour evolution and its key drivers using a cross-regional dataset. A total of 460 monopiles were analysed to obtain 99 local scour depth and their spatial distribution in dependence of on selected hydrodynamic and geological drivers. 100 Understanding scour development is a critical first step in assessing potential environmental impacts. It will help 101 determine whether OWES and entire OWFs contribute to regional sediment mobilization and provide a foundation 102 for future research into the long-term morphological footprint of OWF installations and their broader ecological 103 effects. To contribute to the overarching goal of reducing uncertainty in scour predictions at OWES, this study 104 analyszes field data from 460 monopiles across 9 OWFs, situated in diverse ocean-marine regimes with current 105 velocities from 0.54 m/s to 1.77 m/s (99th percentile), significant wave heights from 1.5 m to 2.7 m (99th 106 percentile), water depths from 5 to 35 m₂ and grain sizes ranging from cohesive sediment (51.54 µm)- to medium 107 gravel (19872 µm). The spatial distribution and variability of relative scour depth across and within these OWFs 108 are determined and correlated with selected hydrodynamic and sedimentological parameters, using Principal 109 Component Analysis (PCA). This analysis aims to (1) identify universal drivers of scour across all sites, (2) assess 110 sediment-specific trends-correlations by grain size (d_{50}) and (3) evaluate site-specific variability at the level of three selected OWFs (Robin Rigg, Lynn and Inner Dowsing, and London Array). The site-specific analysis in 111 112 Section 3.5 assesses the robustness of the global correlations under local conditions and provides insight into how 113 local conditions influence scour behaviour. Collectively, these efforts aim to decrease uncertainty in relative scour 114 depth prediction by assessing the contribution of the main drivers of scour development from multivariable field 115 data.

- 116 This paper is organized as follows: Section 2 describes the study area and methodology in which the methods
- 117 used to obtain the relative scour depth and selected on-site parameters are explained in detail (subsections 2.2 –
- 118 2.5). Additionally, the application of the PCA to identify the primary correlation between these parameters and
- 119 scour development is explained (subsection 2.6). -The results are presented in section 3, followed by discussion
- 120 (section 4) and ending with the conclusions (section 5).

121 2 Study area and methodology

122 **2.1** Study area

- 123 The research area, located in British waters, is illustrated in Figure 1, showing the specific locations of the nine
- 124 studied OWFs. Figure 1A provides a general overview, while Figure 1B pinpoints the positions of the OWFs,
- 125 labeled 1 to 9. These OWFs correspond to Robin Rigg, Barrow, Teesside, Humber Gateway, Lincs, Lynn and
- 126 Inner Dowsing, Greater Gabbard, London Array, and Gunfleet Sands, respectively. Figures 1C and 1D display the
- 99th percentiles of the significant wave heights $(H_{s,99})$ and current velocity magnitudes (U_{99}) at the nine locations,
- 128 respectively.
- 129 Notably, wind farms such as Robin Rigg and Barrow are situated in the Irish Sea, while the remaining seven are
- 130 located in the North Sea at the east coast of the UK (Fig. 1B). Water depths (h) ranging from 5 to 35 m can be
- 131 found across the nine OWFs. Depth data (h) were obtained from EMODNET
- 132 (https://emodnet.ec.europa.eu/en/bathymetry). The OWF located in the shallowest water depth is Robin Rigg
- 133 with h ranging from 1 to 14 m (Fig. 1B). Conversely, the OWF with the deepest water depth is Greater Gabbard
- 134 with h ranging from 21 to 35 m (Fig. 1B).
- 135 The highest and lowest significant wave heights (99th percentile) can be found at Humber Gateway OWF ($H_s = 2.7$
- 136 m) (Fig. 1C-D) and at Gunfleet Sands OWF ($H_s = 1.5$ m), which are located at the mouths of the Humber and
- 137 Thames estuaries (Fig. 1C-D), respectively. Regarding current velocities, the highest value is found at Robin Rigg
- 138 OWF with 1.8 m/s (Fig. 1C-D), while the lowest value is found at Gunfleet Sands OWF with a value of 0.4 m/s
- 139 (Fig. 1C-D).
- 140 Depending on the locations of the OWFs, the seabed conditions vary from sandbanks featuring a variety of
- 141 bedforms to intertidal mudflats. Accordingly, the sediment also varies from silt to coarse and very coarse gravel,
- 142 with the sediment at Teesside OWF consisting of fine and silty sands and that at Humber Gateway consisting of
- 143 sandy gravel and boulders. In contrast, OWFs such as London Array and Greater Gabbard are located in the Outer
- 144 Thames Estuary with sandbanks and channels, while others such as Barrow and Robin Rigg have distinct
- 145 geological features such as megaripples, mudflats, and deposits from different geological eras.

147 2.2 Data description

- 148 Bathymetric datasets from the nine OWFs considered in this study were collected via multibeam echosounder
- 149 (MBES) before, during, and after the construction of the OWFs and were afterwards made available by its their
- 150 operators via the Marine Data Exchange (MDE).
- 151 In total, 460 OWES (of 680 available) with monopiles foundations were analyzed in this study. For the correlation
- 152 between scour and hydrodynamic conditions at the nine studied OWFs, metocean hindcast datasets (i.e., significant

153 wave height (H_s) and velocity magnitude (U)) by the Copernicus Marine Service (CMEMS) 154 (https://marine.copernicus.eu/) were used (CMEMS, 2023a, 2023b).

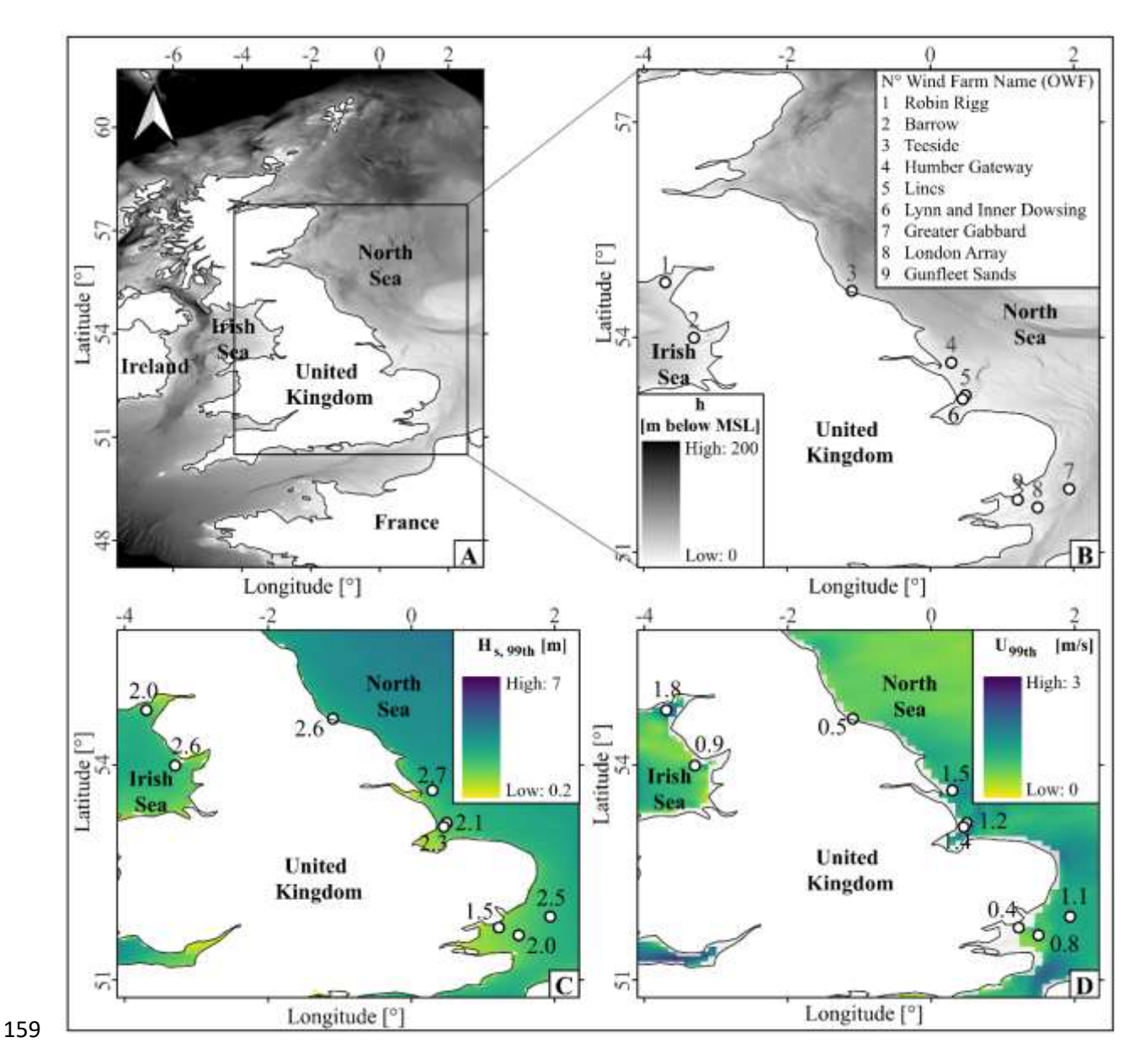


Figure 1: A) Study area. B) Location of the nine studied OWFs. Shown bathymetry data originates from EMODNET (https://emodnet.ec.europa.eu/en/bathymetry). C) 99th percentile of significant wave heights (H_s) based on data for the year 2012. D) 99th percentile of current velocity magnitudes (U) based on data for the year 2012.

Table 1 shows the OWFs considered in this study and provides an overview of their structural characteristics as well as the hydrodynamic and geotechnical site conditions. Pile diameters (*D*) were obtained from Negro et al.

166 (2017), water depths (h) are based on EMODNET (2020), d_{50} represents the median grain diameter of the sediment. The sediment data shown in Table 1 were obtained in Phi units from each OWF's benthic reports, then 167 168 converted to d_{50} values in micrometers (μm) according to Bunte et al. (2001). The scour depth S represents the 169 deepest scour at an individual OWES. The number of OWES varies from 26 OWES installed at Teesside OWF to 170 174 OWES installed at London Array OWF, indicating the different operational scales. For some OWFs, including 171 Lynn and Inner Dowsing, extensive bathymetric data spanning over ten years was available. In contrast, others, 172 such as Humber Gateway, had more limited bathymetric data with a coverage duration of four years. The highest 173 grid resolutions of the bathymetric datasets found at each OWF varied from 0.2 to 0.5 m, with the highest resolution 174 of the bathymetries found at each OWF being used. The earliest bathymetry was collected at Barrow OWF in 175 2005, and the most recent was collected at Lynn and Inner Dowsing in 2017, highlighting the long-term monitoring 176 efforts at the wind farms. However, in this study only scour depth obtained from the pre- and the first post-177 construction bathymetries were considered. -The shortest period between pre_ and post_ bathymetries was found 178 at Lincs OWF, with 377 days between August 2010 and August 2011, while the longest period between scans was 179 detected at Greater Gabbard OWF, with 2902 days (~8 yrs) between June 2005 and May 2013. 180 Furthermore, environmental and hydrodynamic conditions associated with each OWF are also shown in Table 1, 181 which are essential for understanding how different variables contribute to scour around monopiles. These variables include the 99^{th} percentile significant wave height $(H_{s,99})$, representing the average height of the highest 182 183 third of waves. The wave height has a direct influence on the wave-induced current velocity near the seabed and 184 thus strongly determines the bed shear stresses and the formation of the vortex system around the OWES (Sumer & Fredsøe, 2002; Schendel et al., 2018). The 99th percentile current velocity magnitude (U_{99}) indicates the resultant 185 of eastward (u_0) and northward (v_0) tidal flow components $\frac{1}{2}$ those represent the depth-averaged velocity 186 187 magnitude, whereas U_{cr} depicts the critical flow velocity for sediment entrainment. Their ratio, the flow intensity 188 $(U/U_{II})_{99}$ is a key parameter in describing the general sediment mobility and has a large impact (h/D) influences 189 on the formation of the horseshoe vortex in such a way that the size of the horseshoe vortex is reduced as the flow 190 depth decreases, resulting in a reduction in the relative scour depth. At greater relative water depth $h/D \ge 5$) the 191 relative scour depth becomes almost independent of relative water depth (Sumer and Fredsøe, 2002). 192 The Froude number (Fr_{99}) and pile Reynolds number (Re_{99}) are used to characterize the flow conditions around 193 the pile, and their calculations are shown in **T**table 2, Equations 2 and 3. The Froude number indicates whether the 194 flow is dominated by gravitational or inertial forces. With increasing Froude number, stronger inertial forces 195 produce more pronounced pressure gradients at the upstream face of the monopile. Promoting early boundary layer 196 separation and enhances the strength of the horseshoe vortex system near the seabed, which increases local bed 197 shear stress and accelerates sediment erosion. As shown by Hu (2021), these dynamics are key in amplifying scour. 198 Similarly, Corvaro et al. (2015) found that higher Froude numbers lead to larger vortex structures and increased 199 bed shear stress, resulting in deeper equilibrium scour depth. On the other hand, the Reynolds numbers provides 200 information on whether the flow is laminar or turbulent, and determines the characteristics of the vortex system 201 around the pile. 202 Additionally, the Keulegan-Carpenter number (KC_{99}) , which is used to determine the relative influence of drag and inertia forces, the formation of vortices, and the potential for sediment transport (Sumer & Fredsøe, 2002). 203 The mobility parameter $(\theta_{99}/\theta_{cr})$ is considered a key controlling factor for scour, as it represents the degree to 204 205 which the bed shear stress exceeds the critical threshold for reflects the onset of sediment motion under given flow

- 206 conditions (Soulsby, 1997; Whitehouse et al., 2000). The calculations of those two parameters are shown in Ttable
- 207 2, Eequations 9 and 20. The datasets were obtained between pre- and post- construction bathymetries. The data
- 208 was collected over a one-year period, prior to the post-construction bathymetry.²²
- 209 -Dimensionless parameters as given in Table 1 were calculated based on the equations summarized in Table 2.

OWF name	N° of OWES	Pile diamete r D (m)		Scour depth S (m)	Water depth h (m)	D ₅₀ (μm)	Wave height $H_{s,99}$ (m)	Current Velocity U ₉₉ (m/s)	scour			Reynolds number Re ₉₉	Keulegan Carpenter number KC ₉₉	Mobility parameter $\theta_{99}/_{ heta_{cr}}$	Flow intensity $(U/U_{cr})_{99}$
Robin Rigg	60	4.3	Min Max	1.3 10	5 14	167 267	2.36 2.59	1.55 1.77	0.30 2.32	1.03 3.07	0.13 0.23	5.14x10 ⁶ 5.86x10 ⁶	0.99 1.9	15.3 25.4	3.51 4.43
Barrow	30	4.75	Min Max	0.98 6	15 23	138 445	2.43 2.52	0.91 1.11	0.20 1.20	3.67 4.71	0.06 0.08	3.50x10 ⁶ 4.26x10 ⁶	0.34 0.48	4.4 7.2	1.89 2.40
Teesside	26	5	Min Max	0.65 1.62	8 20	51 166	2.52 2.76	0.54 0.54	0.13 0.32	208 3.49	0.04 0.05	2.10x10 ⁶ 2.10x10 ⁶	1.2 1.6	6.1 9.6	1.19 1.29
Humber Gateway	72	4.2	Min Max	0.5 2.51	15 20	5918 1900 0	2.24 2.37	1.51 1.56	0.11 0.59	3.65 4.65	0.11 0.12	4.87x10 ⁶ 5.06x10 ⁶	0.92 1.11	0.4 1.2	0.58 0.99
Lincs	75	5.2	Min Max	0.54 1.92	12 21	505 1982	2.47 2.71	1.07 1.67	0.10 0.38	2.41 3.88	0.08 0.13	4.29x10 ⁶ 6.71x10 ⁶	0.64 1.01	2.6 11.1	1.31 3.12
Lynn and Inner Dowsing	60	4.74	Min Max	0.5 2.35	9 17	684 1950	2.11 2.36	1.30 1.45	0.10 0.49	2.10 3.47	0.11 0.13	4.76x10 ⁶ 5.29x10 ⁶	0.84 1.3	3.2 7.3	1.63 2.53
Greater Gabbard	139	6	Min Max	0.5 4.54	23 35	394 2296	2.41 2.67	1.02 1.22	0.08 0.75	3.50 5.83	0.05 0.07	4.72×10^{6} 5.64×10^{6}	0.18 0.33	1.3 6.1	1.14 2.25
London Array	174	7	Min Max	1.2 9.5	1 27	120 930	1.89 2.36	0.71 0.81	0.21 2.02	0.31 4.67	0.04 0.19	2.56×10^{6} 3.56×10^{6}	0.1 2.3	1.5 32.6	1.14 2.33
Gunfleet Sands	49	4.7	Min Max	0.88 7.73	2 16	146 253	1.52 1.72	0.48 0.86	0.18 1.64	0.54 3.34	0.03 0.09	1.74x10 ⁶ 3.12x10 ⁶	0.45 1.68	2.1 17.6	1.05 2.07

Table 1. Overview of studied OWFs with hydrodynamic and sedimentological site conditions.

Table 2. Calculation of the variables included in the analysis

Variable	Equation	
Current vVelocity magnitude	$U_{99} = (\sqrt{u_0^2 + v_0^2})_{99} \sqrt{u_0^2 + v_0^2}$	(1)
Froude number	$Fr_{99} = \left(\frac{U}{\sqrt{gh}}\right)_{99} \frac{U_{-}}{\sqrt{gh}}$	(2)
Pile Reynolds number	$Re_{99} = \left(\frac{UD}{v}\right)_{99} \frac{U_D}{v}$	(3)
Dimensionless -grain size	$D_* = \left(\frac{\rho g}{v^2}\right)^{\frac{1}{3}} d_{50}$	(4)
Critical Shields	$\theta_{cr} = \frac{0.3}{1 + 1.2D_*} + 0.55(1 - \exp(-0.02D_*))$	(5)
U_{cr}	$U_{cr} = 7 * \left(\frac{h}{d_{50}}\right)^{\frac{1}{7}} (g(s-1)d_{50}\theta_{cr})^{0.5}$	(6)
Flow intensity	$(\frac{U}{U_{cr}})_{99}$	(7)
Zero crossing period (T_z)	$\frac{T_p}{1.28}$	(8a)
Natural period (T_n)	$T_n = \sqrt{\frac{h}{g}}$	(8b)
A_{t}	$A_t = (6500 + \left(0.56 + 15.54 \frac{T_n}{T_z}\right)^6)^{1/6}$	(8c)
RMS velocity (U _{rms})	$U_{rms} = 0.25 \frac{H}{T_n (1 + \left(A_t \frac{T_n^2}{T_z}\right))^3}$	(8d)
Wave-induced velocity (U_m)	$U_m = \sqrt{2} \ U_{rms}$	(8e)
Keulegan-Carpenter number (KC)	$KC_{99} = \left(\frac{U_m T_p}{D}\right)_{99} \frac{U_m T_p}{D}$	(9)
Roughness related to d_{50} (ks)	$k_s = 2.5d_{50}$	(10)
Amplitude of wave orbital motion at the bed (A)	$A = \frac{U_m T_p}{2\pi}$	(11)
shear velocity (U_f)	$A = \frac{U_m T_p}{2\pi}$ $U_f = \frac{U}{6.0 + 2.5 \ln\left(\frac{h}{k_s}\right)}$	(12)

wave friction factor
$$(f_w)$$

$$f_w = \begin{cases} 0.32 \left(\frac{A}{k_s}\right)^{-0.8}, & \frac{A}{k_s} < 2.92 \end{cases}$$

$$0.237 \left(\frac{A}{k_s}\right)^{-0.52}, & 2.92 \le \frac{A}{k_s} < 727 \end{cases}$$

$$0.04 \left(\frac{A}{k_s}\right)^{-0.25}, & \frac{A}{k_s} \ge 727 \end{cases}$$

$$\alpha = atan2(u_0, v_0) - D_w$$

$$\alpha = atan2(u_0, v_0)$$

- The values assumed for all OWFs sites are:
- 218 $\rho_s = 2650 \, kg/m^3$, (sediment density, based on Soulsby, 1997), $\rho_w = 1027 \, kg/m^3$ (water density), $\nu_w = 1000 \, kg/m^3$
- 219 $1.3x10^{-6}m^2/s$ (kinematic viscosity), $g = 9.8 m/s^2$ (gravitational acceleration).
- Where ρ_s is the sediment density, based on Soulsby (1997). ρ_w is the water density, v is the kinematic viscosity
- 221 and g the gravitational acceleration. Equation 4 was calculated based on van Rijn (1984), where D_{*} is the non-
- 222 dimensional grain diameter that is used to calculate the critical Shields parameter (θ_{cr}), which represents the
- 223 threshold for initiation of motion at the bed, as proposed by Soulsby (1997).
- Equation 5 is taken from Soulsby and Whitehouse (1997), where s ($s = \frac{\rho_s}{\rho_w}$) represents the specific gravity of
- 225 sediment grains. The d_{50} represents the median sediment grain size.
- 226 In equation 18, the maximum bed shear stress value (τ_{max}) was calculated following Roulund et al. (2016), which
- 227 builds upon Soulsby (1997) by combining current- and wave-induced shear stress through a directional correction.
- 228 Shields parameter (θ_{99}) is derived using equation 19, based on the maximum bed shear stress (τ_{max}) under
- 229 combined wave and current conditions. The Keulegan-Carpenter number is defined in equation 10, where T_p is
- 230 the peak wave period and D the monopile diameter.
- 231 Equation 20 provides the calculation of the mobility parameter to assess sediment mobility, providing a
- dimensionless indicator of whether the hydrodynamic forcing was sufficient to initiate sediment motion. All
- 233 relevant equations are summarized in **T**table 2.

235 2.3 Pre-processing of bathymetric data

-Figure 2 shows the workflow used in this study, starting with the acquisition of bathymetric datasets, originally obtained from the Marine Data Exchange, and their conversion to Ordnance Datum Newlyn (ODN). This was followed by the generation of 100_m x 100_m tiles for each available bathymetric dataset, centered on each turbine location. If bathymetric scans with different spatial resolutions were available for the same date, only the one with the highest resolution was used. In addition, some turbine locations could not be further analysed due to missing pre-construction scans or poor data quality. Tiles with more than 50% empty cells were discarded because a high percentage of missing data increases the likelihood that important areas, such as the scour region, are poorly captured. Tests were conducted with lower missing cell thresholds (10% and 25%), but even with 50% missing data, valuable information for scour analysis was retained. Using a stricter 25% threshold, too many tiles were lost, including those that still contained useful data. As a result, 460 OWES across the nine OWFs were analysed in this study.

The difference in bed elevation at turbine sites between the pre-construction (Fig 2.A) and post-construction surveys (Fig 2.B), was used for extracting scour information. The deepest scour at each turbine site was then extracted from the difference plot (Figure 2.C). A detailed description of this part of the workflow is provided in

section 2.4.

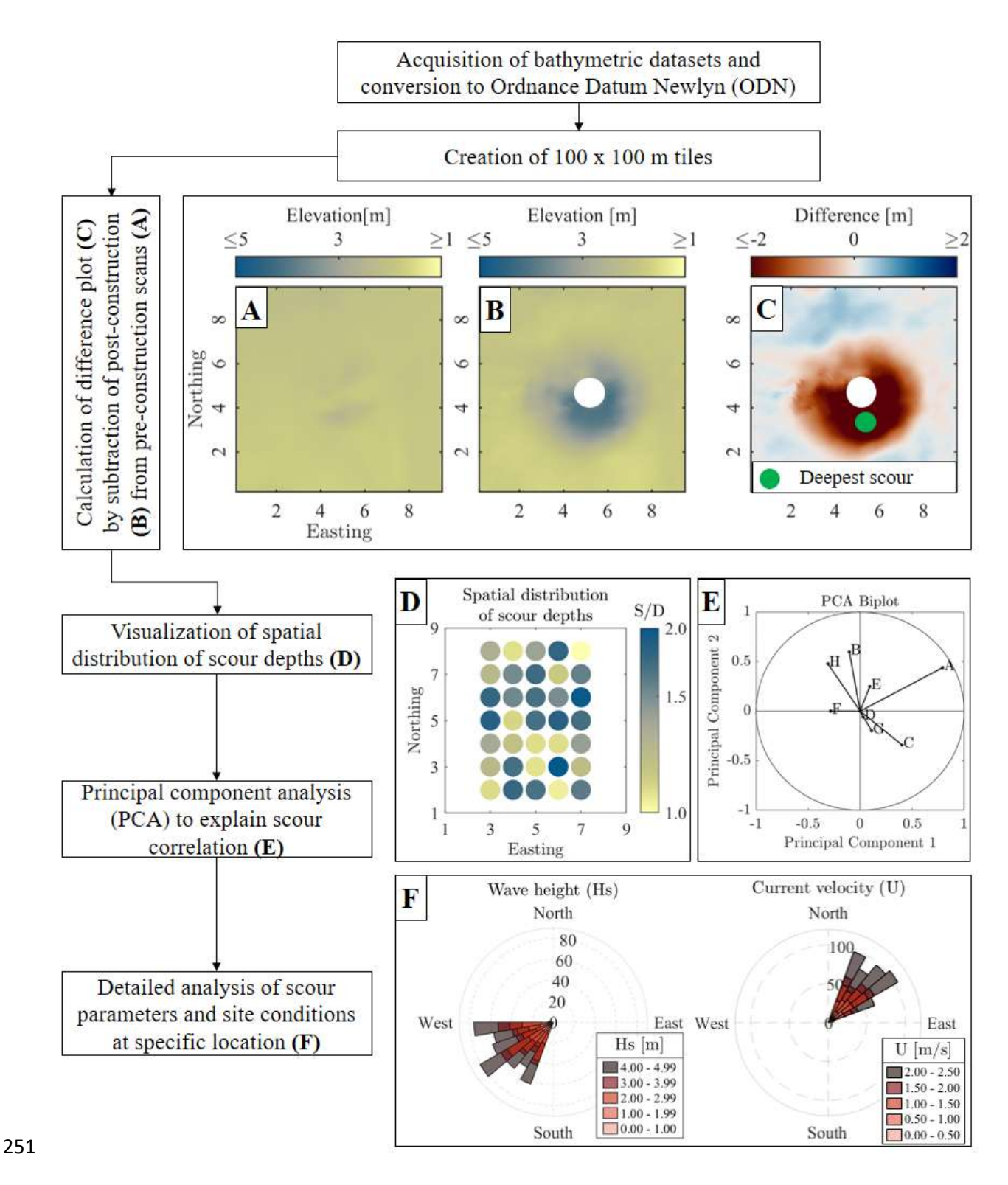


Figure 2: General workflow and methodology used to assess the scour distribution and evolution as well as the correlation between scour parameters and site conditions. A) Pre-installation scan. B) Post-installation scan. C) Difference plot after subtraction of B from -A. D) Map of spatial distribution of relative scour depth. E) Principal Component Analysis (PCA). F) Site conditions of wave heights and current velocities.

256 2.4 Calculation of scour parameters

First, to eliminate outliers, a threshold based on the 99th percentile was used to filter out extreme values, ensuring that outliers did not skew subsequent analyses or visualizations. Subsequently, to address potential offsets between

pre- and post-construction, a median filter was applied to both datasets. The difference in medians, excluding the presumed scour area, was considered the offset. This offset was then applied while calculating the difference plot between the pre- and post-construction bathymetries (Fig. 2A-C). To remove additional outliers close to the turbine, an area equivalent to 110% of the pile's footprint area was excluded from the center of the difference plot. The deepest scour depth (see green dot in Fig. 2C) was then extracted from the difference plot (Fig. 2C). The calculated relative scour depth were then visualized to show the spatial distribution across the nine OWFs (Fig. 2D).

2.5 Principal component analysis (PCA)

267 In the case of field data, the correlation of the scour process with hydrodynamic and geotechnical variables is 268 complicated by the simultaneous change of several of these variables. In order to reduce the complexity and 269 simplify this multivariate problem, PCA was used in a next step (Fig. 2.E). PCA works by transforming the data 270 into a set of new variables called principal components, which are linear combinations of the original variables 271 (Jolliffe & Cadima, 2016). These components are ordered based on how much variance they explain, with the first 272 principal component (PC1) explaining the maximum variance in the data, followed by the second principal 273 component (PC2). -Each component also has an eigenvalue, which shows the amount of variation it captures. 274 Generally, the PCA is able to handle lots of independent variables and helps to simplify the data without losing 275 important information (Harasti, 2022).

In this study, the PCA was applied to a dataset of 692 OWES, including 460 from our analysis and an additional

276277

266

278 232 OWES from London Array and Thanet OWF, based on Melling's (2015) data. The PCA was then performed 279 using eight independent variables that contributed to the principal components. Those dimensionless variables were the relative water depth (h/D), Keulegan-Carpenter number (KC_{99}) , mobility parameter $(\theta_{99}/\theta_{cr})$, Reynolds 280 number (Re_{99}) , Froude number (Fr_{99}) , relative sediment size $({}^{d_{50}}/_{D} \frac{D/d_{50}}{D})$, flow intensity $(({}^{U}/_{U_{rr}})_{99})$, and the 281 relative scour depth (S/D). Following this, the data was organized into a matrix, with each row representing a 282 283 specific OWES and each column representing a selected dimensionless variable. All the variables were extracted 284 as representative values specific to the OWES, with the focus on the 99th percentile to capture extreme 285 hydrodynamic conditions. Scour processes are more likely to occur in these extreme conditions because maximum 286 scour depth usually develops during storm-induced events, rather than under mean or median values. 287 Subsequently, the variables were standardised to ensure the comparability of the results. 288 In some studies, the PCA is used for reducing the number of dimensions (Harasti, 2022), or to help develop 289 predictive models grouped by soil classes (Annad, 2023). However, the aim of this study was to keep all the 290 principal components. This approach enabled the full exploration of the interdependence between physical drivers 291 and scour response across sites. To interpret the relationships among the variables, a principal component analysis 292 biplot was generated (Gabriel et al., 1971). In the biplot, variables are represented as vectors, and the angle between 293 vectors indicates the degree of correlation. The strength of the correlation was quantified using the cosine of the 294 angle (Jolliffe & Cadima, 2016), enabling us to assess the strength of association between each variable and scour variability across different OWFs sites. Similar to previous studies that applied PCA for parameter selection in 295

bridge pier or scour formula development (Harasti, 2022; Annad, 2023), this multivariate analysis provides a

297 clearer understanding of which parameters dominate the scour process under real offshore conditions

An additional approach to reducing the complexity of multivariate datasets is to initially group the data based on a selected key variable. Accordingly, the PCA was also applied to the dataset after it had been grouped by grain size (d_{50} diameter) classes (Annad et al., 2021), given that the sediment characteristics of the seabed play a significant role in local scour (Qi et al., 2016). This approach facilitated a more precise estimation of local scour,

302 thereby reducing uncertainties related to sediment.

303 3 Results

304

305

319

3.1 Spatial distribution of relative scour depth

306 To illustrate the variability in relative scour depth between the nine studied OWFs and within single OWFs, Figure 307 3 shows the spatial distribution of relative scour depth. There are clear differences between OWFs in both the 308 magnitude and variability of relative scour depth. For example, at OWF Robin Rigg (Figure 3.A), the highest relative scour depth were identified, the values range from S/D=0.29 to S/D=2.49. This OWF is characteriszed 309 310 by fine and medium sands. In contrast, the smallest relative scour depth occurred at the OWF of Lynn and Inner 311 Dowsing (Figure 3.F), with values from S/D=0.12 to S/D=0.92, which is possibly linked to coarse sands presented 312 at this site. Furthermore, the highest variability ($\sigma = 0.44$) in relative scour depth were detected at OWF London 313 Array (Figure 3.H) and Barrow (Figure 3.B), likely influenced by the complex seabed morphologies and sediment 314 compositions in these areas. On the other hand, the significant variability at London Array may be explained by 315 the presence of the Long Sand and Kentish Knock sandbank. This illustrates how different site characteristics can 316 result in various scour distributions, even within a single OWF. 317 The remaining OWFs showed relatively low relative scour depth and little spatial variability, even though site conditions were significantly different, as indicated by their seabed conditions from very fine sand for Teesside 318

(Figure 3.C) to coarse and very coarse gravel for Humber Gateway (Figure 3.D).

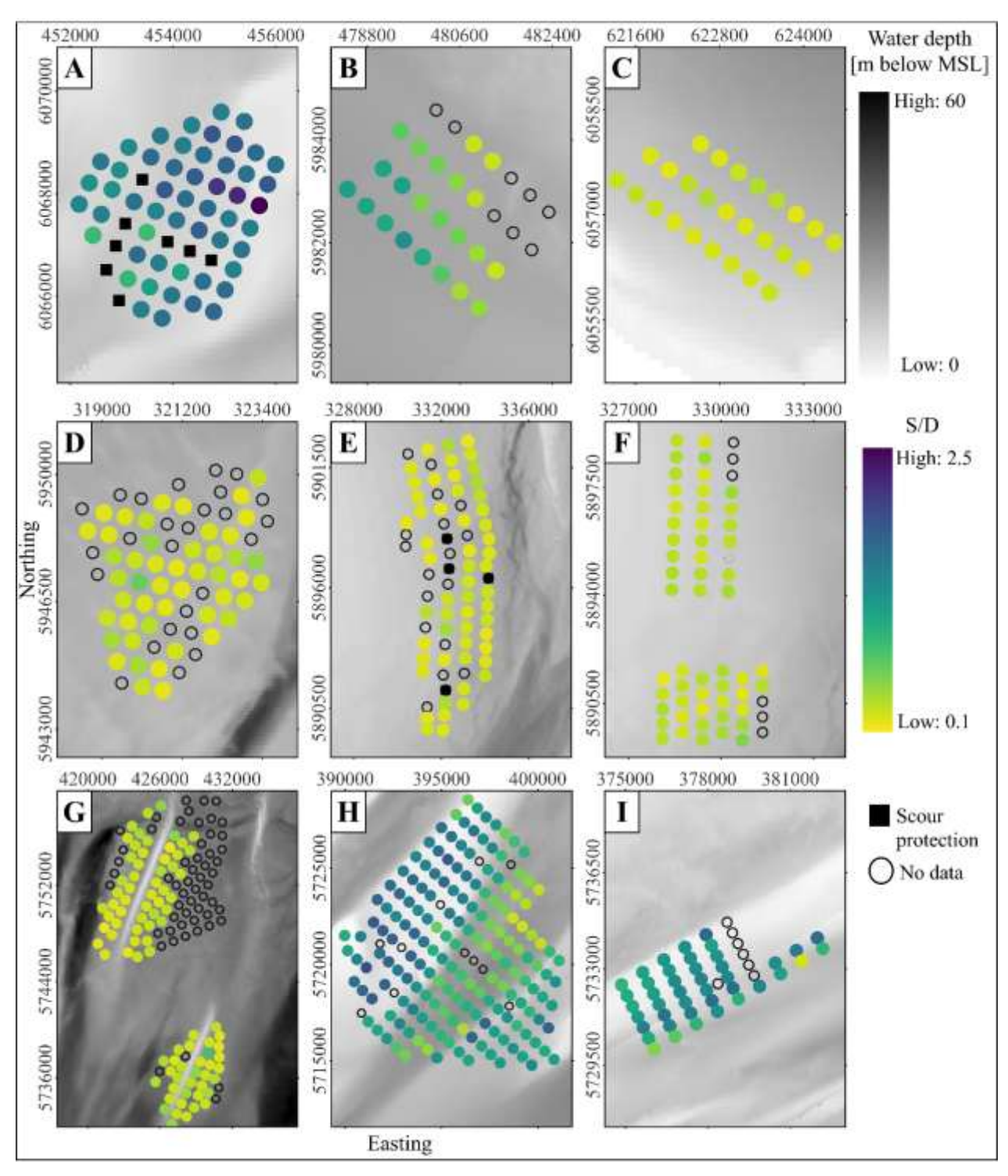


Figure 3: Spatial distribution of relative scour depth at the nine studied OWFs. Lettersred markers (A-I) denote the locations of Robin Rigg, Barrow, Teesside, Humber Gateway, Lincs, Lynn and Inner Dowsing, Greater Gabbard, London Array, and Gunfleet Sands OWFs, respectively. The upper colourmbarp represents water depth, with darker shades indicating deeper water. The lower colourmap indicates relative scour depth, with darker blue colour indicating the largest scour. Black filled squares represent OWES with scour protection, while empty circles denote missing data. Shown bathymetry data originates from EMODNET (589).https://emodnet.ec.europa.eu/en/bathymetry).

329 3.2 Principal Ceomponent Analysis (PCA)

330

331

332

333

334

335

336

337

338

339

340

341

342

343

344

345

346

347

348

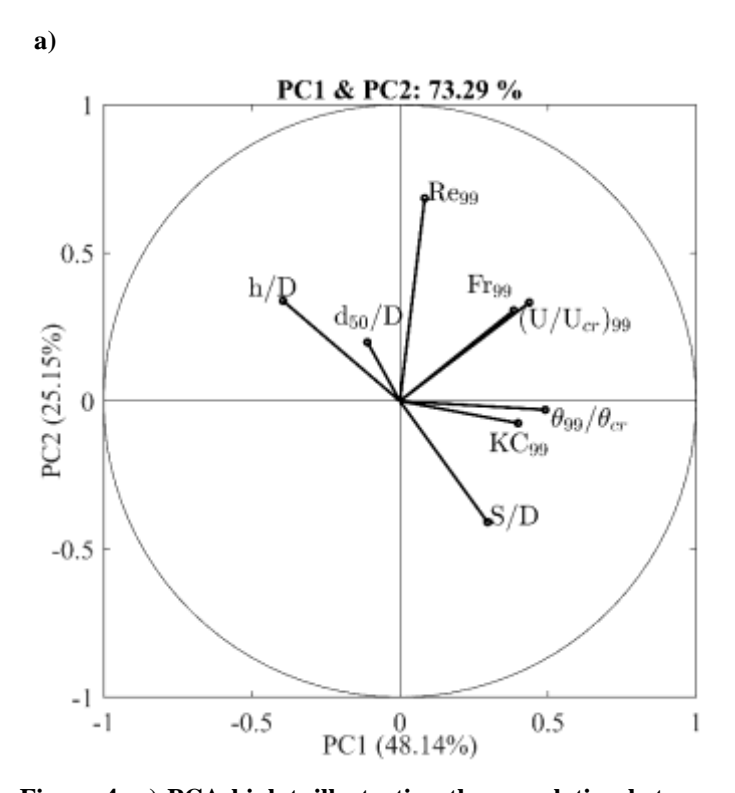
349

350

351

The analysis of Figure 3 reveals notable variations in relative scour depth across individual OWFs. This variance underscores the need for a more detailed examination of specific wind farm characteristics to identify the drivers of scour. To this end, a PCA was conducted to correlate relative scour depth and selected parameters by identifying and quantifying their relationships. The PCA biplot presented in Figure 4 illustrates these correlations between relative scour depth and the studied variables and provides a comprehensive view of how different factors interact and influence relative scour depth.

b)



Variables	θ to S/D	Cosine-based
		Correlation
		with S/D
d_{50} H/D	165.59 <u>173</u>	0.9 <u>9</u> 6
$\frac{D/d_{50}}{h}$	<u>35.53</u> <u>166</u>	0. <u>97</u> 81
KC ₉₉	35.91 <u>43</u>	0. <u>72</u> 80
$ heta_{99}/ heta_{cr}$	43.60 <u>50</u>	0.7 <mark>2</mark> 0
Re ₉₉	13 <u>7</u> 4. 21	0.6 <u>3</u> 5
$(U/U_{cr}\frac{U}{U_{er}})_{99}$	83.84 <u>92</u>	0. <u>46</u> 11
Fr_{99}	<u>91</u> 84.17	0.402

Figure 4: a) PCA biplot, illustrating the correlation between variables and relative scour depth-. b) The table detailing the angles between the relative scour depth and the other variables (in degrees), along with the magnitude cosine-based correlation (values from 0 to 1), where values closer to 1 indicates stronger correlation. Boldface highlights the variables with the strongest correlation with relative scour depth. As shown in the biplot, PC1 and PC2 account for 743.0329% of the variation in the data set. This high percentage indicates that these two components capture most of the significant patterns in the data, allowing for a meaningful interpretation of the relationships among the variables. In the biplot, each vector stands for a variable, with the direction and magnitude of the vector reflecting its contribution to the principal components. The variables that contribute the most to the variance in PC1 are the mobility parameter, the Froude number, and Keulegan Carpenter number, with shares of 0.4898, 0.44193, and 0.411439, respectively. In contrast, the variance in PC2 is primarily explained by the pile Reynolds number, the relative grain sizewater depth and the Froude number, with shares of 0.628, -0.48934, and 0.31683, respectively. This significant contribution of the mobility parameter, the Froude number, and the Keulegan Carpenter number to PC1 suggests that variations in these hydrodynamic parameters are critical in shaping the principal dynamics of the dataset. The table (Fig. 4b) next to the biplot provides further insight by showing the angular distances between the S/D vector and each of the other variables, as well as their respective correlation coefficients. One of the key observations is that relative the relative scour depth has the

352 strongest negative correlation of 0.996 with the relative water depthgrain size. This highlights the critical influence 353 of sediment size on scouring processes, even though it does not account for much of the variance captured by the 354 first two principal components. This observation can be explained by the underlying physical processes that affect scour depths. As noted by Whitehouse (2010) for non-cohesive sediments, larger sediment sizes are more resistant 355 356 to erosion, resulting in reduced scour depths. Therefore, while relative grain size is strongly correlated with scour 357 depths, it does not explain the broader variability in the data that is influenced by other factors. The next strongest 358 correlation is with the relative water depth with a correlation factor of 0.97, which underscores the critical role of 359 water depth in governing scour intensity. Shallower relative depths concentrate flow energy at the bed, intensifying 360 near-bed velocities and shear stresses that promote deeper scour holes (Smith & McLean, 1977; Whitehouse, 361 2010). The next strongest correlation is with the relative grain size with a correlation factor of 0.81. This suggests 362 that as the relative grain size increases, relative scour depth also tends to increase. This trend is in line with the 363 functional dependence of relative scour depth on relative grain size as observed by Sheppard et al. (1995, 1999). 364 This positive trend may be due to increased turbulence caused by larger bed roughness elements or the initiation 365 of larger scale scour processes around coarser particles under certain flow conditions (Whitehouse, 2010). 366 Furthermore, a significant positive correlation was found with the Keulegan-Carpenter number with a correlation 367 factor of 0.8172, indicating the importance of oscillatory flow conditions in scour development. Higher Keulegan 368 Carpenter number directly leads to higher relative scour depth (Sumer and Fredsoe, 2002). This is driven by the 369 onset of the horseshoe vortex and lee-wake eddy shedding (Sumer et al., 1992b; Zanke et al., 2011), with increased 370 permanence of the horseshoe vortex and amplification of bed shear stresses at higher KC values (Sumer et al., 371 1997). In addition, the mobility parameter exhibits a strong positive correlation (0.740) with the relative scour 372 depth. The mobility parameter quantifies the instantaneous capacity of the flow to exceed the entrainment 373 threshold, driving rapid sediment entrainment when significantly above unity (Soulsby, 1997; van Rijn, 1993). 374 Variables such as the pile Reynolds number, the flow intensity, and the Froude number, although less correlated 375 with relative scour depth, contribute more to the total variance. This suggests that these flow-related variables 376 influence relative scour depth through more complex or non-linear interactions with other hydrodynamic 377 conditions and sediment characteristics. 378 Given that the initial PCA analysis indicates the strongest negative correlation between the relative grain size and 379 relative scour depth, and Ssince seabed sediment characteristics play a significant role to local scour (Qi et al., 380 2016), the PCA was applied again to the same dataset but pre-clustered into different soil classes (Annad et al. 381 2021).- By reducing the uncertainties related to grain size (d_{50}) , this analysis should provide a better estimation of 382 the local scour. This classification also facilitates the identification of parameters that are more influential in 383 estimating scour for specific soil classes, rather than uniformly across different types. After the clustering, six soil 384 classes were obtained: cohesive sediment ($d_{50} \le 63 \mu m$) with 5 data points, fine sand ($63 \le d_{50} < 200 \mu m$) with 385 203 data points, medium sand ($200 \le d_{50} < 630 \ \mu m$) with 249 data points, coarse sand ($630 \le d_{50} < 2000 \ \mu m$) with 170 data points, fine gravel (2000 $\leq d_{50} < 6300 \ \mu m$) with 18 data points, and medium gravel ($d_{50} \geq 6300 \ \mu m$) 386 387 μm) with 49 data points.

3.3 Principal Ceomponent Analysis (PCA) by clustered soil classes

388

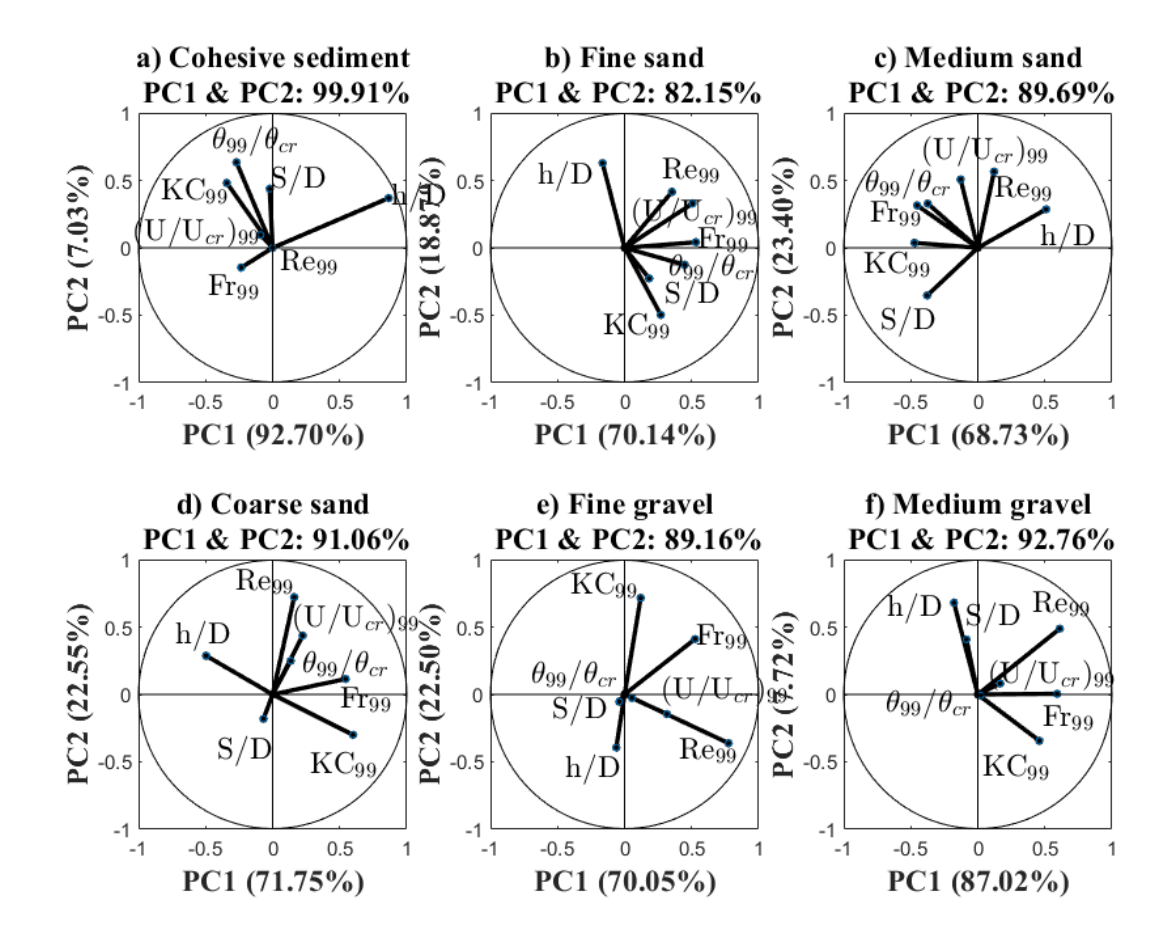


Figure 5: PCA correlation by clustered soil classes based in the grain size (d_{50}) , -remaining parameters that are shown in the biplots are explained in data description (section 2.2). a) Cohesive sediment ($d_{50} \le 63 \, \mu m$). b) Fine sand (63 $\leq d_{50} <$ -200 μm). c) Medium sand (200 $\leq d_{50} <$ -630 μm). d) Coarse sand (630 $\leq d_{50} <$ 2000 μ m). e) Fine gravel (2000 $\leq d_{50} <$ -6300 μ m). f) Medium gravel ($d_{50} \geq$ -6300 μ m). Clustering of the grain size (d_{50}) was based on Annad et. al. (2021). Building on the initial PCA analysis, which emphasized the significant influence of grain size on relative scour depth-, a more detailed investigation was conducted by categorizing the dataset into six soil classes: cohesive sediment ($d_{50} \le 63 \ \mu m$) with 5 data points, fine sand ($63 \le d_{50} < 200 \ \mu m$) with 203 data points, medium sand $(200 \le d_{50} < 630 \ \mu m)$ with 249 data points, coarse sand $(630 \le d_{50} < 2000 \ \mu m)$ with 170 data points, fine gravel $(2000 \le d_{50} < 6300 \ \mu m)$ with 18 data points, and medium gravel $(d_{50} \ge 6300 \ \mu m)$ with 49 data points. Figure 5 shows PCA biplots for each soil class illustrating the relationships between relative scour depth the relative water depth, the Keulegan-Carpenter number, the mobility parameter, the pile Reynolds number, the flow intensity and the Froude number. The first two principal components (PC1 and PC2) explain between 82.15 % and 99.91% -of the variance within each class, thus describing more of the variance in comparison to when the PCA was applied to all data. Data complexity seems to be greatly reduced by just removing the effect of sediment. In the cohesive

391

392

393

394

395

396

397

398

399

400

401

402

403

404

405

406

407

sediment soil class (Figure 5a), relative scour depth is positively correlated with the mobility parameter. However,

408 the calculation of the mobility parameter might contain larger uncertainties for cohesive soils (Soulsby, 1997), so 409 the results should be treated with caution. 410 In contrast, relative water depth has a strong negative correlation with relative scour depth in fine sand (Figure 5b) 411 and medium sand (Figure 5c). This indicates that as relative water depth increases, relative scour depth tends to 412 decrease in these finer soil classes. From a physical view, Melling (2015) found out that in similar substrates, 413 relative scour depth agree well between different geographic locations and showed that OWES located in sandy 414 sediments exhibit a strong influence of relative water depth on scour, suggesting geotechnical factors are less 415 influential in coarser sediments. Although the observation that relative scour depth decreases as relative water 416 depth increases might initially seem counterintuitive. This behaviour is best explained through the transition 417 between shallow-water and deep-water flow regimes. As flow approaches a pile, stagnation pressure develops on 418 its upstream face, causing the flow to separate into an up-flow and a down-flow component. The down-flow is 419 directed toward the bed and promotes the formation of a horseshoe vortex. Flow separation occurs at the stagnation 420 point, defined as the location of maximum energy from the approaching flow at the pile face. The energy of the 421 approach flow consists of hydrostatic and kinetic components, whose vertical distribution is governed by the 422 boundary layer. In shallow water, the kinetic component dominates over hydrostatic pressure, resulting in a 423 stagnation point located higher up the pile, near the water surface. This enhances down-flow and vortex activity, 424 intensifying scour processes (Melville, 2008). Additionally, shallower water often features thinner boundary layers 425 with higher velocity gradients near the seabed, potentially leading to greater bed shear stresses and increased 426 sediment mobility. In contrast, in deeper water, hydrostatic pressure becomes more influential, leading to a more 427 uniform pressure field across the pile face and shifting the stagnation point closer to the bed. This results in weaker 428 down-flow and reduced vortex strength, thereby diminishing the scour depth (FHWA, 2012; Harris & Whitehouse, 429 2014). Furthermore, Link and Zanke (2004) observed that maximum relative scour depth tends to develop more 430 slowly and reach lower values in deeper water depth, even under constant average flow velocity, due to reduced 431 shear velocity over the undisturbed bed. This highlights that the relationship between relative water depth and 432 scour is not necessarily linear. 433 The dynamics observed in coarse sand (Figure 5d) and fine gravel (Figure 5e) are different from the finer 434 sediments. In these classes, the flow intensity and the Froude number show significant negative correlations with 435 relative scour depth, indicating that higher values of these parameters correspond to reduced relative scour depth. 436 However, these soil classes are also characterized by comparatively small relative scour depth, which makes the 437 relationship less prominent. 438 For medium gravel (Figure 5f), relative water depth has a positive correlation with relative scour depth, meaning 439 that greater relative water depth are is associated with greater relative scour depth in coarser sediments. The data 440 points in the cluster can be attributed to the Humber Gateway OWF, which is the only OWF that features clear-441 water conditions. Given the large grain sizes, a smaller influence of flow parameters on the variability of relative

443

444

442

3.4 Correlation of scour depth with main drivers

scour depth should be expected.

Following the PCA (Figure 5), which identified the primary variables influencing relative scour depth across soil classes, a Pearson correlation analysis was performed to quantify the strength and direction of these relationships.

447 Figure 6 shows the Pearson correlation results for each cluster and the variable with the strongest correlation, with

the red lines representing the linear regression fit and the correlation coefficients shown in red text. The Pearson correlation was calculated by the following equation:

450
$$R = \frac{\sum (x_i - \bar{x})(y_i - \bar{y})}{\sqrt{\sum (x_i - \bar{x})^2 \sum (y_i - \bar{y})}} \dots (9)$$

Considering the small number of data points in this sediment cluster, relative scour depth at locations with cohesive sediments (Fig. 6a) shows a moderate correlation between scour with the mobility parameter. For the fine and medium sand clusters, the PCA revealed a similarly strong dependence of relative scour depth on relative water depth. Plotting relative scour depth against relative water depth now shows a clearer trend-correlation and hence dependence for the medium sand sites (Fig. 6c) than for the fine sand sites (Fig. 6b). The Pearson coefficients of -0.57 and -0.86 confirm this difference in the dependence of relative scour depth on relative water depth. The correlations of the fine and medium sand clusters are supported by a larger number of data points, increasing the reliability of the findings.

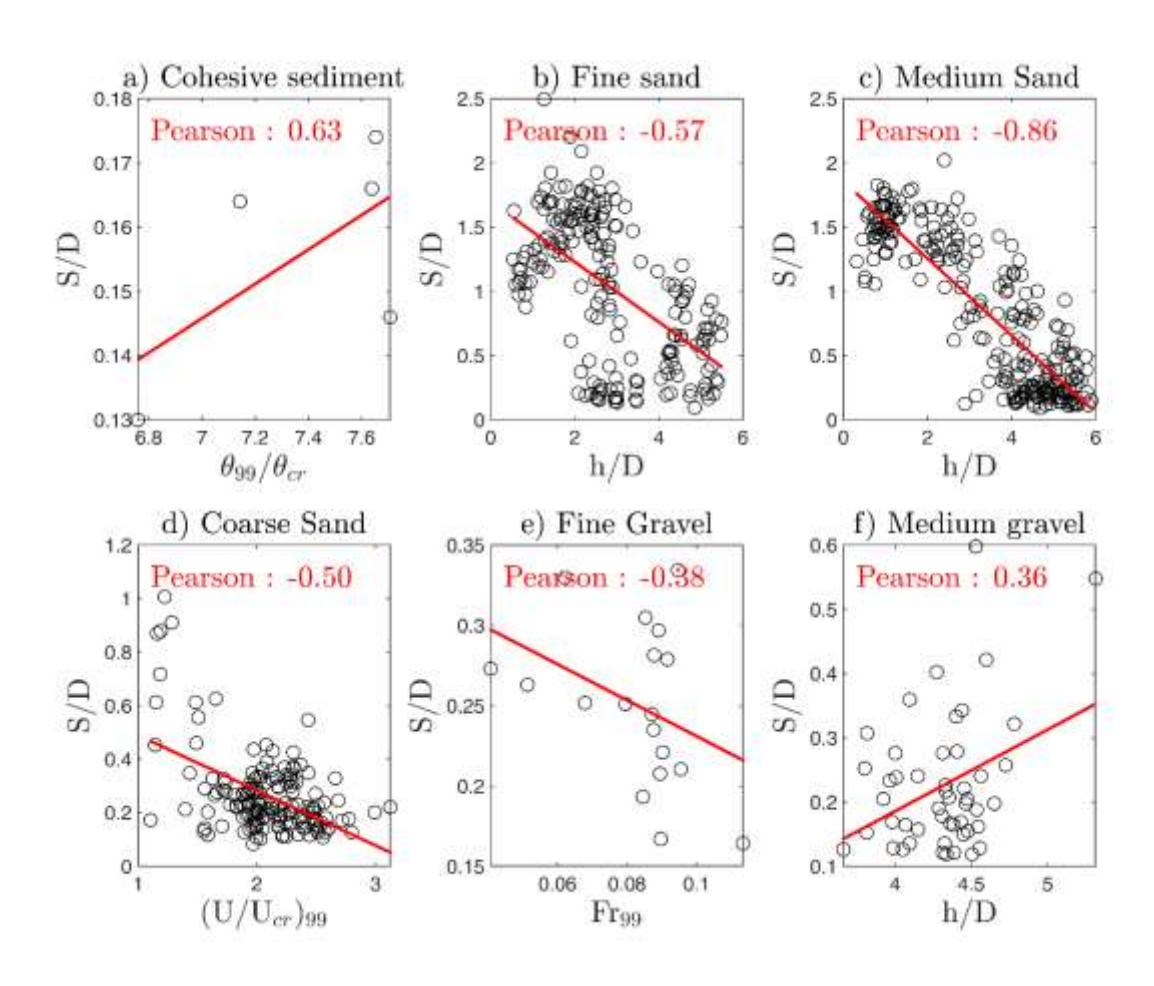


Figure 6: Pearson correlation of representative variables obtained by PCA analysis with relative scour depth across different soil classes. -a) Cohesive sediment ($d_{50} \le 63 \ \mu m$). b) Fine sand ($63 \le d_{50} < 200 \ \mu m$). c) Medium sand ($200 \le d_{50} < -630 \ \mu m$). d) Coarse sand ($630 \le d_{50} < 2000 \ \mu m$). e) Fine gravel ($2000 \le d_{50} < 6300 \ \mu m$). f) Medium gravel ($d_{50} \ge 6300 \ \mu m$). For the coarse sand (Figure 6d), the PCA analysis revealed a negative correlation between relative scour depth and

flow intensity. This result directly aligns with the established understanding of live-bed scour behaviour in coarse-

grained sediments. Once flow intensity surpasses the critical threshold ($(U/U_{cr})_{99} > 1$), the sediment mobilizes, 466 467 establishing live-bed conditions. In such scenarios, the development of large, well-defined scour holes is 468 consistently observed to be suppressed. This suppression occurs because the continuous transport and 469 replenishment of sediment into the scour region actively works against deep erosion. This dynamic equilibrium of 470 the seabed results in shallower, or inherently more unstable, scour holes when compared to clear-water conditions. 471 In clear-water, where sediment remains immobile, scouring is driven purely by flow-induced vortex action around 472 the structure (Sumer & Fredsøe, 2002; Whitehouse et al., 2011). Consequently, the negative correlation observed 473 in this soil class accurately reflects the inherent limitation of scour growth under the highly mobile conditions 474 characteristic of coarse sandy beds. 475 For fine gravel (Figure 6e), the PCA suggests a correlation between relative scour depth and the Froude number, 476 but this is difficult to confirm visually due to the small sample size and narrow Froude number range. Since relative 477 scour depth is comparatively small in this class, relationships are less clear, and parameters like Froude number 478 come to the foreground that were not as prominent in finer sediments. A broader distribution of Froude 479 number values would be necessary to confirm this more conclusively. 480 Finally, medium gravel (Figure 6f) displays a positive correlation between relative scour depth and relative water 481 depth, with a Pearson coefficient of 0.36. This indicates that larger relative water depth correspond to increased 482 scour depth, although the range of this increment remains small (between S/D = 0.1 and S/= 0.4). This variation 483 in scour depth is small compared to the correlations observed in fine and medium sands, where changes in relative 484 water depth yield more pronounced differences in relative scour depth. The smaller impact in medium gravel -may 485 be attributed to the generally greater resistance of larger sediments to scour, even with increasing relative water 486 depth. 487 The most significant correlations emerge from the fine sand (Figure 6b) and medium sand (Figure 6c), where 488 strong negative correlations between relative scour depth and relative water depth are observed. This suggests that 489 significant scour occurs in shallower waters with finer sediments. Such findings highlight the importance of 490 relative water depth as a key factor influencing scour processes in specific sediment types, emphasizing that scour 491 management and predictions for offshore structures should take sediment characteristics and relative water depth 492 into account. These results are consistent with the studies from Melling (2015) and Harris and Whitehouse (2014), 493 which also show a decrease in relative scour depth in finer sediments as relative water depth increase. This negative 494 correlation can be explained by the reduction in bed shear stress with increasing relative water depth, which limits 495 sediment mobilization, particularly in fine and medium sands (Sumer & Fredsøe, 2002; Fredsøe & Sumer, 2014). 496 However, those results disagree with experimental work where scour around a monopile weakens with reducing 497 relative water depth (e.g. May and Willoughby, 1990; Whitehouse, 1998). Consequently, relative water depth is included as a parameter in many empirical formulas, especially in for scour around bridge piles with limited water 498 499 depth (eg., Laursen, 1963; Hancu, 1971; Breusers et al., 1977; May and Willoughby, 1990; Richardson et al., 500 2001). Besides that, these insights from field data are critical for the accurate assessment and planning of offshore infrastructure installations, particularly in regions with varying sediment characteristics.

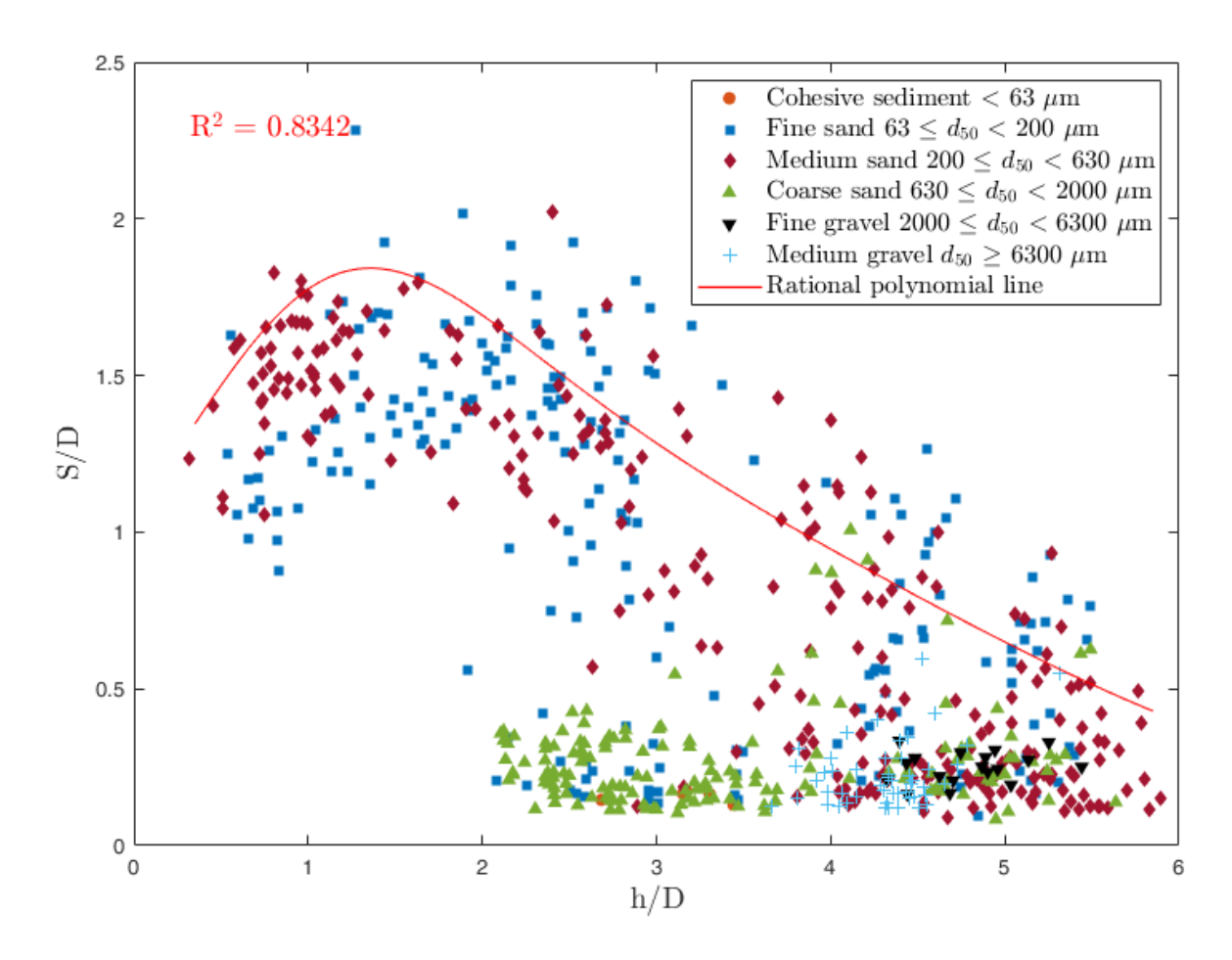


Figure 7: Relative scour depth vs relative water depth, and soil classes. The solid red curve represents a red rational polynomial line represents a trend correlation to based on the course of the 99th percentile of relative scour depth. Data points for London Array and Thanet OWFs are included from Melling (2015). Figure 7 summarizes the findings from the PCA analysis (Figure 4) by plotting the relationship between the relative scour depth and the relative water depth. Relative water depth has shown to be the one of the parameters with the largest correlation influencing relative scour depth. However, it should be noted that relative water depth has a

direct effect on other hydrodynamic parameters. For example, not only is the Froude number formed with the water depth, but relative water depth also significantly determines the potential influence of waves on the development of scour, which in this study has also been considered by the Keulegan–Carpenter number. Therefore, it remains unclear whether the influence of relative water depth on relative scour depth is a direct causal factor or an indicator of broader changes in hydrodynamic conditions. Nevertheless, Figure 7 illustrates the comprehensive correlation between the relative scour depth and the relative water depth with the differently colored points markers (colour and shape) representing the studied soils classes. The solid red curve shows a correlation between relative scour depths across all relative water depths, independent of sediment class. This curve was systematically developed by fitting a rational polynomial function to the 99th percentile values of relative scour depth, computed

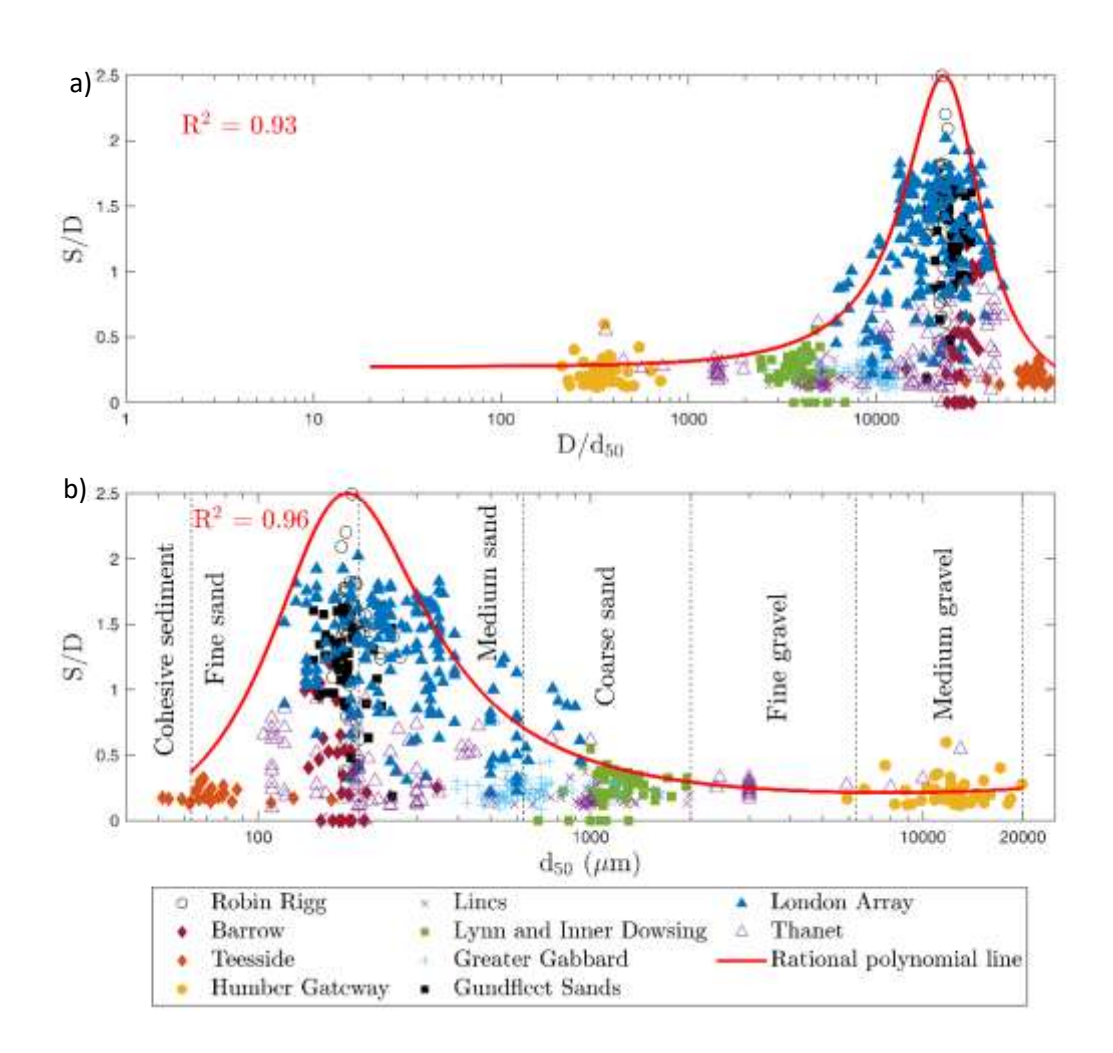
within uniform relative water depth intervals (e.g., 0.1).

The trend_correlation_observed in Figures 6b and 6c is reaffirmed in Figure 7. A distinct relationship exists between the relative scour depth and relative water depth in these two sediment types, i.e. both fine sand $(63 \le d_{50} < 200 \mu m)$ and medium sand $(200 \le d_{50} < 630 \mu m)$ show that the relative scour depth decreases with increasing relative

water depth. This <u>correlation</u>trend appearing throughout the bigger dataset emphasizes a strong negative correlation between relative water depth and relative scour depth for those soil classes. This behaviour is consistent with findings from previous analyses that identified relative water depth as a critical factor in shaping scour dynamics (Whitehouse et al., 2010 and Melling, 2015).

In contrast, for sediments with median grain diameters above coarse sands ($d_{50} \ge 630 \, \mu m$) the relative scour depth remains relatively constant and shows little variability. Figure 7 suggests a generally stable relationship between relative scour depth and relative water depth for these soil classes, where changes in relative water depth do not significantly alter relative scour depth. However, there are a few exceptions. For example, some locations with coarse sand located in deeper water exhibit unexpectedly large relative scour depth. These outliers might stem from site-specific conditions such as dynamic sandbanks and highly variable bathymetry, as seen at the London Array OWF (Sturt et al., 2009). These unique environments, characterised by flow recirculation and sediment mobility, can lead to deviations from expected scour behaviour (Melling, 2015). The results for fine and medium sands suggest a potential influence of relative water depth in reducing relative scour depth. Although these results are preliminary, they provide a first step in understanding how offshore wind OWES could affect sediment redistribution in regions dominated by these sediment types and small relative water depth.





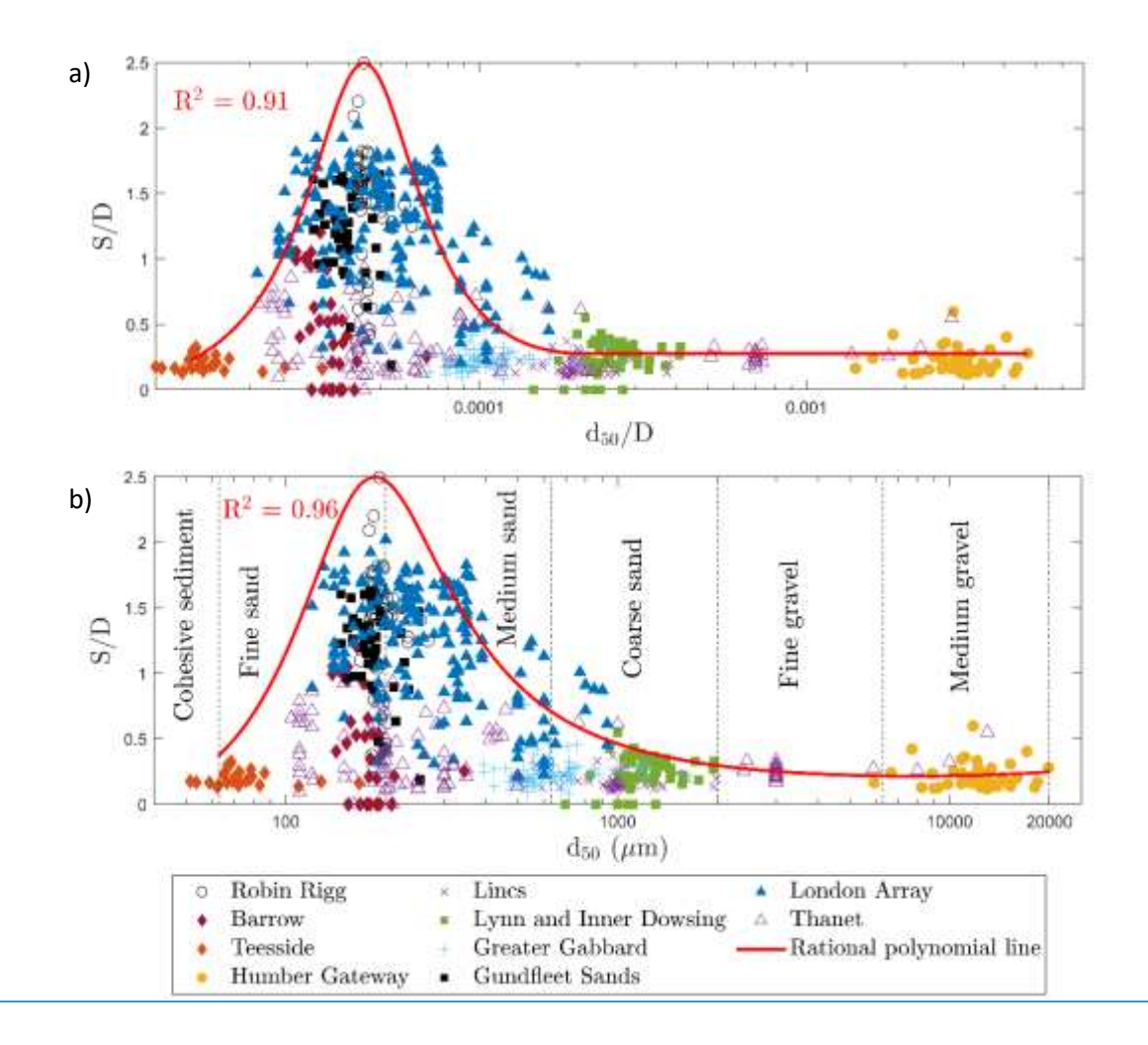


Figure 8: Relative scour depth against (a) the relative grain size, and (b) grain size. The solid red curves represent red the rational polynomial line fits to the 99th percentile of relative scour depth, line gives the approximate upper limit of S/D, based on the course of the 99th percentile, for various relative grain size and grain size various d_{50} . Data points for London Array and Thanet OWFs are included from Melling (2015).

Figure 8a summarizes the findings from the PCA analysis (Figure 4) by plotting the relationship between the relative scour depth and relative grain size across all the sampled locations. Figure 8b is also shown here to support figure 8a by representing the data in terms of the grain size, allowing the comparison of dimensional and non-dimensional relative grain size. Figures 8a and 8b, reveals no clear trend between relative scour depth and relative grain size, indicating that the dimensionless grain size ratio alone does not adequately capture the relationship between sediment properties and scour depth in field data. Sheppard et al. (2004) observed a clear trend of S/D decreasing for $\frac{D}{d_{50}} > 50$ in laboratory experiments, which is not consistent with our results. However, field data show much weaker dependence due to natural variability in sediment structure and hydrodynamic forcing.

On the other hand, Figure 8b illustrates a discernible trend correlation where the largest relative scour depth occurs predominantly in fine to medium sands (R²= 0.840791 and R²=0.96), as indicated by the rational polynomial line which approximates the upper limit of relative scour depth for various relative grain size (Figure 8a) and grain size (Figure 8b). Similar to the correlation presented in Figure 7, this curve approximate upper limit of S/D and it was derived by fitting a rational polynomial function to the 99th percentile values of relative scour depth, computed

within uniform interval of relative grain size (e.g., 0.00001) and grain size (e.g., 25 µm). The trend correlation shown in Fig. 8b is figures 8a and 8b are well explained. In general, the mobility potential of the sediments decreases with increasing grain size, which leads to lower relative scour depth for coarser sediments. Very fine sediments, on the other hand, are subject to the influence of cohesion forces that reduce their erodibility, which also leads to lower relative scour depth. Therefore, fine and medium sandy sediments have the largest scour potential, which is reflected in the data of Fig. 8b. The different symbols represent the OWF, highlighting the geographic spread and variability within the dataset. However, it is important to note that most of the data points fall within the range of fine to medium sands, potentially skewing the interpretation.

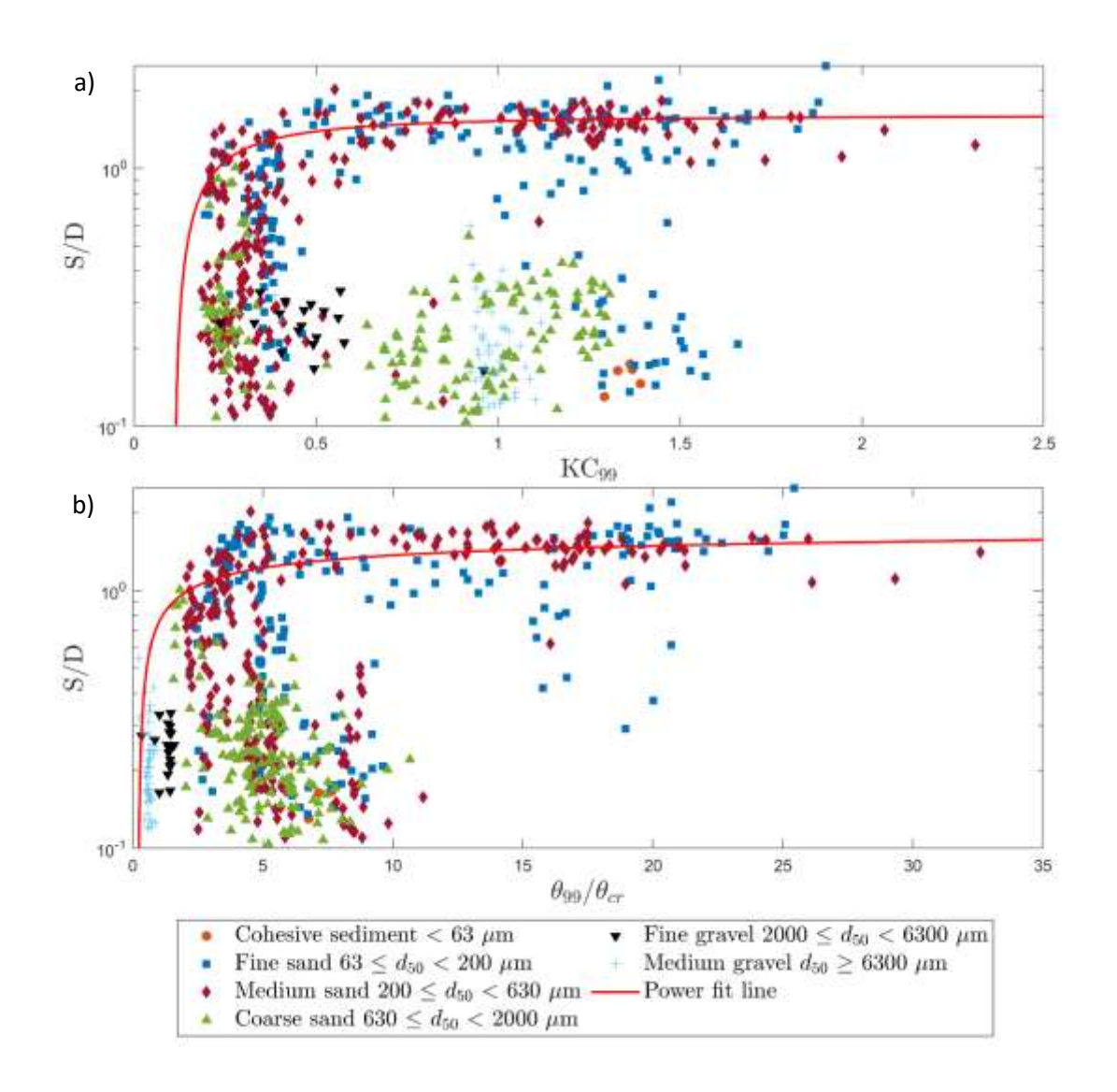


Figure 9: Relative scour depth against the a) Keulegan-Carpenter number and b) the mobility parameter.

The red line gives the power fit line based on the 99th percentile of the data of relative scour depth for various grain size d₅₀. Data points for London Array and Thanet OWFs are included from Melling (2015).

575 The third and fourth parameters, that correlate with the relative scour depth, are the Keulegan-Carpenter number 576 and the mobility parameter as identified by the PCA. Figure 9a shows the correlation between the relative scour 577 depth and the Keulegan-Carpenter number, revealing a distinct increase of relative scour depth with increasing Keulegan-Carpenter number up to $KC_{99} = 0.5$. Above this value, relative scour depth shows little variation with 578 579 further increase of the Keulegan-Carpenter number, which reaches a maximum value of 2.5 in this field dataset. 580 Those results are generally consistent with findings from previous studies (e.g., Qu et al., 2024; Sumer & Fredsøe, 581 2002), which indicate that scour development is strongly dependent on KC_{99} at lower values, but becomes less 582 sensitive as KC_{99} increases. However, experimental studies often focus on wave regimes with KC numbers greater 583 than 6, since it has been established that this is the threshold for generating a horseshoe vortex. Despite considering 584 the 99th percentile of KC numbers over the time period in question, the KC numbers are much smaller for the field 585 conditions presented herein. This strengthens the argument for further scour research to focus on boundary 586 conditions with low KC values. 587 Figure 9b shows the correlation between relative scour depth and mobility parameter, comparing the Shields 588 parameter with its critical threshold for sediment motion, and revealing a distinct increase of relative scour depth 589 with increasing mobility parameter up to approximately $\theta_{99}/\theta_{cr}=5$. At higher mobility values (typically above 5– 590 10), the increase in scour depth tends to stabilize. This trendcorrelation aligns with experimental observations from 591 Sumer et al. (2013), Chiew (1984), and others, which describe similar stabilization of scour depth under fully 592 mobile conditions. Notably, the response also varies with sediment type: coarser sediments exhibit low relative 593 scour depth values even at high mobility ratios, likely due to their higher resistance to entrainment and potential 594 armoring effects. In contrast, finer sediments (e.g., $d_{50} < 200 \,\mu m$) show a steeper increase in scour depth, 595 reflecting their greater susceptibility to hydrodynamic conditions. 596 Overall, Figure 9a and 9b emphasize the nonlinear and sediment-dependent nature of scour formation. The 597 separation of trends correlations by soil class supports the need for sediment-specific scour prediction models, as 598 also suggested in previous studies (e.g., Whitehouse et al., 2011; Sumer & Fredsøe, 2002). The results provide 599 empirical evidence of this dependency using field-scale data, bridging a critical gap between controlled 600 experiments and real-world conditions.

601

602

3.5 Detailed analysis of scour patterns for selected OWFs

Following the observed overall trend_correlation shown in Figure 7, this section moves on to examine scour patterns within individual OWFs, such as Robin Rigg, Lynn and Inner Dowsing, and London Array. This specific analysis will assess whether the global relationship between relative scour depth d_{50} , and relative water depth holds under the unique environmental conditions of each site. This section aims to further our understanding of the dynamics between sediment characteristics and scour processes by a detailed analysis of the variation within each wind farm to determine if these global correlations are consistent at the local scale or if there are deviations due to site-specific factors.

610 3.5.1 Robin Rigg OWF

Robin Rigg is presented and discussed in this section, as this OWF has the largest overall relative scour depth of all the OWFs. This detailed analysis will help to investigate whether the negative correlation between relative

613 scour depth and relative water depth observed globally in Figure 7 holds true under variable geotechnical 614 conditions, taking into account that sediment grain sizes range from fine to medium sands. 615 Figure 10 shows the distribution of relative scour depth at Robin Rigg in relation to the variable geotechnical and 616 hydrodynamic site conditions. This sequence begins with Figure 9A, showing the spatial distribution of scours 617 measured one year after turbine installation. A significant variation in relative scour depth in different areas of the 618 OWF can be observed, with the deeper relative scour depth mainly located in the north-eastern part, particularly 619 around OWES D7, C6, B5 and B4, which are located in the shallowest waters. Figure 10B shows the spatial 620 distribution of the median grain diameter d_{50} in the uppermost sediment layer in 2005, with sediment sizes 621 predominantly in the range of fine to middle sand (182 µm to 268 µm). OWES in areas with finer sands, such as 622 D4, D5, and D6, are observed to generally experience the large scour, consistent with previous observations by 623 Whitehouse (2006) that finer sand substrates are more susceptible to scour. 624 Figure 10C shows the correlation of relative scour depth and relative water depth, classified by coloured points 625 which represent sediment grain size from figure 9B. Contrary to the clear negative correlation between relative 626 scour depth and relative water depth -observed globally in Figure 8, Figure 10C shows a wide distribution of data 627 points with no clear trendcorrelation, suggesting that local factors in addition to relative water depth and sediment 628 type have an influence on scour at this site. 629 For additional insight, Figures 10D and 10E show the distribution of the directions of significant wave heights, as 630 well as the directions of current velocity magnitudes one-year period, prior the post scan. The highest wave heights 631 came predominantly from the southwest, which should influence sediment mobility and thus scour structures along 632 this direction and especially in shallow relative water depth where wave-induced shear stresses should be higher. 633 Similarly, the tidal current, with its main directions of south-west and north-east, should result in a change in 634 relative scour depth along this main axis. However, a clear trendcorrelation of relative scour depth changing in 635 this direction is not given for Robin Rigg.

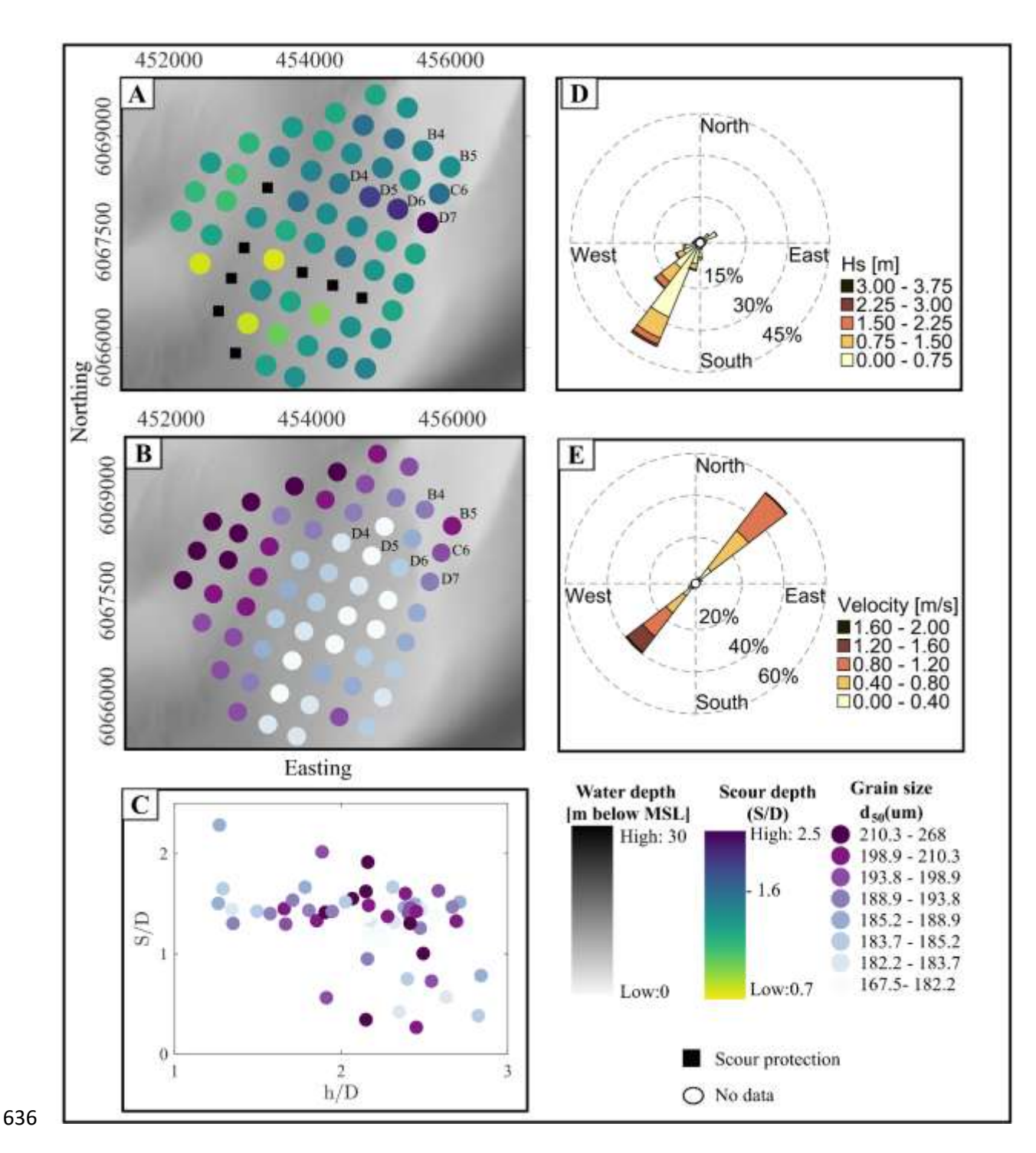


Figure 10: A) Spatial distribution of relative scour depth from 2008-2009 at Robin Rigg OWF. -B) Grain-size distribution. C) Relative scour depth vs relative water depth, and grain size classification. D) Significant wave heights and E) Current velocities.

This comprehensive analysis using Figures 10A to 10E shows that while correlations obtained from global findings provide a useful baseline for understanding scour, the actual scour observed at Robin Rigg does not necessarily follow those correlations. While the distribution of relative scour depth appears to be strongly influenced by local environmental conditions such as sediment type, waves and currents, the dominant influence among these cannot be clearly identified, rather the distribution of relative scour depth appears to be due to the interaction of all influences.

The discrepancies between the local scour behaviour at Robin Rigg and the broader correlations observed in Figure winderscore the need for site-specific assessments. Such detailed analyses are critical to the development of effective scour management and mitigation strategies tailored to the unique conditions of each offshore wind farm.

3.5.2 Lynn and Inner Dowsing OWF

Lynn and Inner Dowsing was chosen as a further example as this OWF had the lowest relative scour depth of all the OWFs investigated and is also characteriszed by coarse to very coarse sands. -Figure 11 provides the same analysis as Figure 10 by providing insight into how local conditions compare to the global <u>correlation trend</u> seen in Figure 7. Figure 10A shows the spatial distribution of relative scour depth measured from 2007 to 2010. Figure 11A shows that the largest relative scour depth are mainly concentrated in the Inner Dowsing area, especially around OWES ID1, ID2, ID8, ID9, ID12, ID24, and ID30. Except for turbine L21, which has the deepest relative scour depth in the entire wind farm and which is located at the south_eastern end. The significant relative scour depth observed at certain locations (e.g., D30, L21) are related to cable exposure (EGS Ltd, 2012; EGS Ltd, 2013), while smaller relative scour depth are more common in the southern region. Overall, the spatial distribution shows a slight <u>trend-correlation</u> of increasing relative scour depth from south to north.

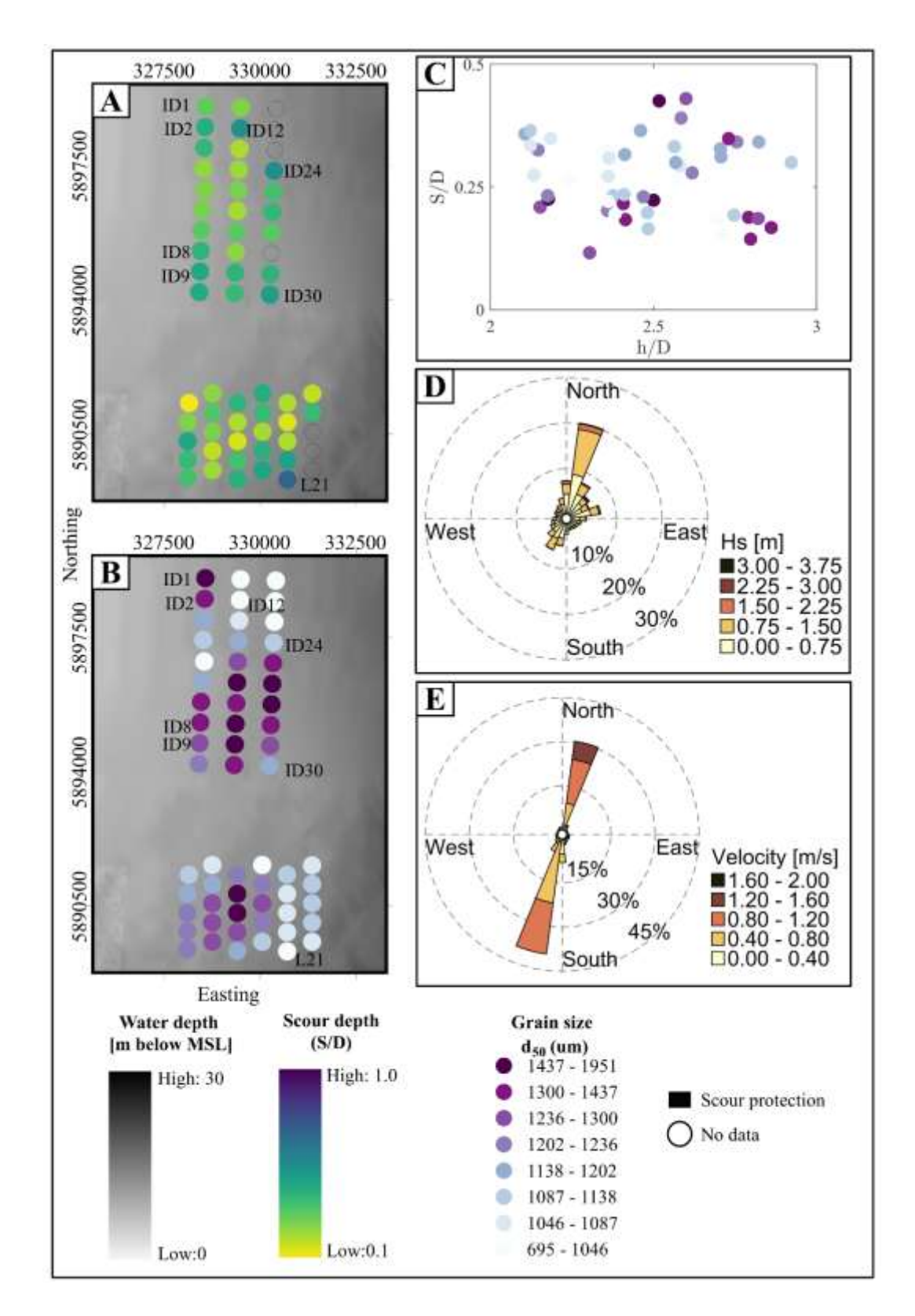


Figure 11: A) Spatial distribution of relative scour depth at Lynn and Inner Dowsing OWF from 2007-2010. B) Grain-size distribution. C) Relative scour depth vs relative water depth, and grain size classification. D) Significant wave heights and E) Current velocities. Continuing with the spatial overview, Figure 11B introduces the spatial distribution of d_{50} median grain sizes, which shows a range from coarse to very coarse sands (695 to 1951 μm). The correlation between relative scour

negative correlation as seen globally in Figure <u>87</u>, suggesting that additional local factors may significantly influence relative scour depth.

Consequently, the significant wave heights and current velocities from hindcast data are shown in Figure 10D and 10E. The highest wave heights, observed from the northeast, and strong tidal currents flowing from southwest to northeast, highlight the dynamic environmental forces at play. The presence of the largest relative scour depth in the Inner Dowsing area align with the direction of the highest tidal current velocities (Fig. 11E) recorded in the northeast part₂ as well the main direction of waves. Therefore, the direction of both tidal current and waves likely play a significant role for the scour development in this wind farms, as the seabed conditions and relative water depth locally do not exhibit a distinct correlation.

678 3.5.3 London Array OWF

Following the previous results, the analysis for London Array OWF shows a wide range of relative scour depth from S/D = 0.2 to S/D = 2.1. This variability differs markedly from the consistently larger relative scour depth observed at Robin Rigg and the limited maximum depth of up to S/D = 1.0 at Lynn and Inner Dowsing. "The area of London Array OWF is characteriszed by an alternating pattern of deep channels (Black Deep, Knock Deep) and sandbanks (Long Sands, Kentish Knock). These topographic features significantly contribute to the local scour patterns. Water depth at this site range from 0 to 30 m, with Long Sands known for its significant variations in bed elevation but general stability of position. Meanwhile, Knock Deep is notable for its eastward shift over time, which has widened the channel and maintained a constant bed level.

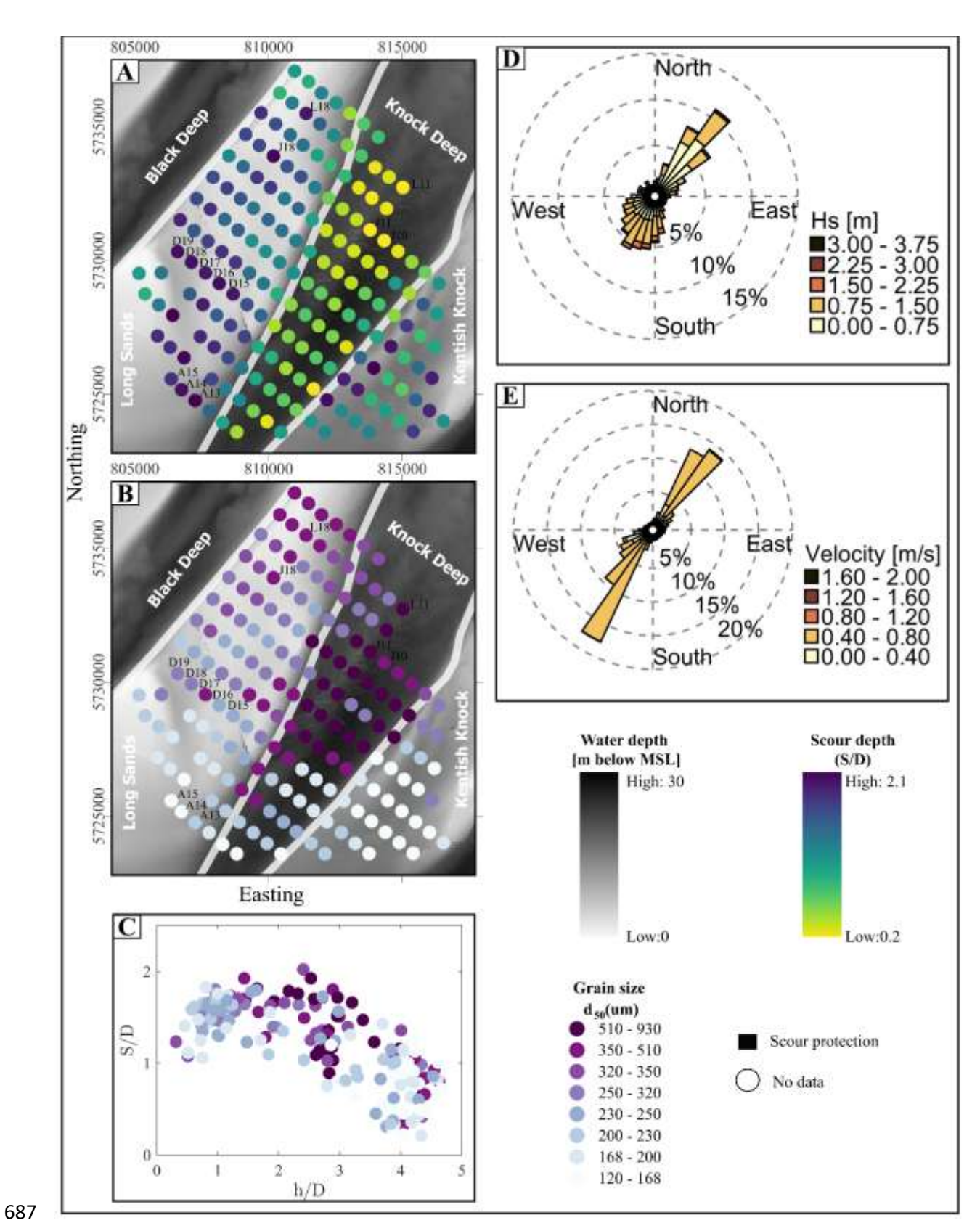


Figure 12: A) Spatial distribution of relative scour depth at London Array OWF from 2010-2014. -B) Grain-size distribution. C) Relative scour depth vs relative water depth, and Grain size classification. D) Significant wave heights and E) Current velocities. Relative scour depth and grain size data are used from Melling (2015)

693 the underlying topography, with significantly greater relative scour depth on the sand banks compared to the 694 channel. Additionally, a trend-correlation of increasing relative scour depth is observed from northeast to 695 southwest, which is particularly notable in the channel area. The smallest scour is observed in the northern part of 696 Knock Deep with a ratio of S/D = 0.2 and the largest in the southern part of Long Sands with S/D = 2.1. The 697 differences in relative scour depth can be derived directly from the seabed topography, with greatest average 698 relative scour depth found in the Long Sands with S/D = 1.53, followed by Kentish Knock (S/D = 1.37), and 699 then Knock Deep (S/D = 0.77) with the smallest average. The sediment distribution across this OWF, shown in 700 Figures 12B, ranges from very fine to coarse sands. Coarse sands can be found in Knock Deep, where generally 701 the smallest relative scour depth are seen (e.g., L11, J10 and J11).- Furthermore, the largest relative scour depth 702 are noticed in the southern part of Long Sands (e.g. A13-A15, D15-D19, J18 and L18), where the sediment varies 703 from very fine to fine medium sands. There is therefore a reasonable correlation between grain size and relative 704 scour depth, which is consistent with the previously observed global correlation trend. Additionally, Figures 12C 705 shows a negative correlation between relative scour depth and relative water depth aligning with the global 706 correlation trend observed in Figure §7, i.e. that shallower relative water depth can be associated with deeper scour, 707 while deeper waters tend to have reduced relative scour depth. This trendcorrelation may be explained by the 708 findings of Hjort (1975), who demonstrated that bed shear stress decreases with increasing relative water depth for 709 the same flow and structure diameter, potentially leading to reduced scour at greater depth. However, as the relative 710 water depth in the London Array OWF changes simultaneously with the sediments, i.e. coarser grained sediments 711 are present in the deeper water depth of Knock Deep, the cause of the different relative scour depth cannot be 712 clearly attributed to either the sediments or the water depth. -Other hydrodynamic, environmental, and topographic 713 factors also play a critical role in shaping these patterns at this OWF, underscoring the complexity of the influences 714 involved. Significant wave heights and current velocities, as shown in figures 12D and 12E, provide important insights into 716 the scour dynamics at the London Array. These figures show that, in addition to relative water depth and sediment 717 grain sizes, wave and current dynamics might be critical factors at this wind farm. The predominant direction of 718 both waves and currents is northeast to southwest, consistent with the estuarine influence of the area, where river 719 discharge also significantly affects hydrodynamic conditions. This influence is particularly evident at the Long 720 Sands and Kentish Knock sandbanks, which are shaped by the combined action of waves and currents (London 721 Array Ltd, 2005). 722 Figures 12D shows that the highest wave heights are observed coming from the northeast, with values exceeding 723 3.0 m, and lower wave heights propagating from the southwest. This gradient in wave height suggests a correlation 724 with increased relative scour depth in regions exposed to higher wave energy, suggesting a strong link between 725 wave dynamics and seabed modification. However, estimated KC99 numbers remained relatively low across most 726 sites, indicating limited wave-induced orbital motion near the seabed. This suggests that wave action plays a 727 secondary role in scour development compared to currents. Similarly, Figure 12E highlights a larger number of strong currents coming from the southeast. These higher velocities correspond to areas with more pronounced 729 relative scour depth, highlighting the role of strong currents in influencing sediment transport and depositional

In Figure 12A, the distribution of relative scour depth shows that the variation in scour is strongly influenced by

692

730

731732

In addition, the local tidal dynamics vary significantly across the wind farm, with the flood tide dominating the

- 733 is due to the sheltering effect of the sandbanks, which are slightly offset from the orientation of the ebb tide, and
- 734 is particularly pronounced at Long Sands (London Array Ltd, 2005). The interplay of river discharge, wind stress,
- 735 tidal surge and density driven currents follow the pathways created by the existing topography, further
- 736 complicating the hydrodynamic environment and its effect on scour at the London Array OWF.
- 737 After analyszing the relative scour depth at 9 wind farms and with different ranges of relative scour depth, the
- 738 variation of relative scour depth can also be noticed in individual OWFs, as in the case for London Array OWF.

740

741

4. Discussion

4.1 Discussion of implications for scour predictions for OWFs

- 742 Overall, this study extends the investigation of scour dynamics to a regional scale by analysing correlations
- 743 between relative scour depth and site conditions across multiple OWFs to identify consistent scour patterns and
- 744 correlations. The PCA analysis highlights a significant negative correlation between relative scour depth with
- 745 relative water depth, suggesting that relative water depth plays a critical role in scour processes, confirming the
- 746 correlations observed with previous Whitehouse et al. (2010) and Melling (2015) for field data. The decrease of
- 747 the relative scour depth with decreasing relative water depth seems unexpected and contradicts common scour
- 748 prediction approaches such as- Breusers et al. (1977), which however are often derived for flow conditions with
- 749 shallow relative water depth. Harris and Whitehouse (2014) argued that in deeper water, a weaker downflow and
- 750 hence a weaker horseshoe vortex can be expected, ultimately leading to smaller scour depth. -This finding implies
- 751 that scour prediction approaches should place greater emphasis on relative water depth, particularly in offshore
- 752 environments where deeper flow conditions dominate.
- 753 A second notable correlation was identified between the relative scour depth with the relative grain size. This
- 754 broad correlation, consistent across different geographic locations and environmental conditions, reinforces the
- 755 fundamental role of sediment size in scour processes, as documented in the extensive work of Vanhellemont et al.
- 756 (2014) and Rivier et al. (2016).
- 757 However, the analysis also indicates that the sediment erodibility alone cannot fully account for the observed
- 758 variability in relative scour depth. The PCA analysis further reveals a -positive correlation between the relative
- 759 scour depth and both the Keulegan Carpenter number and the sediment mobility parameter. The strong positive
- 760 correlation with KC₉₉ supports previous studies (Sumer and Fredsoe, 2001; Qu, 2024), highlighting the importance
- 761 of flow unsteadiness that is typical in tidal and wave-dominated environments. -Similarly, the positive association
- 762 with the mobility parameter underscores its relevance as a key indicator of sediment entrainment and a useful
- 763 metric for distinguishing between different sediment transport regimes.
- 764 These findings underscore a complex dynamic that is frequently oversimplified in existing models. The results
- 765 indicate a necessity to incorporate nonlinear hydrodynamic models into scour prediction frameworks. The results
- 766 of the PCA reveal the necessity for a diversified approach to the modelling of scour in complex field conditions,
- 767 which extends beyond the scope of traditional uniform applications.
- 768 This analysis demonstrates that individual OWFs exhibit unique environmental and sediment conditions, which
- 769 can either amplify or moderate broader correlations. The London Array OWFs serves as a prime example of the
- 770 predictive reliability of observed regional correlations, as local data closely mirrors general correlations.
- 771 Conversely, sites such as Robin Rigg and Lynn and Inner Dowsing exhibit deviations from these correlations due
- 772 to their distinct sediment compositions and hydrodynamic conditions, underscoring the necessity for site-specific

adjustments to scour prediction models. These findings underscore the intricacy of employing global models on a local scale and underscore the significance of site-specific data in validating and refining these models to enhance their accuracy and applicability.

4.2 Discussion of Llimitations and future research

- Although this study provides a detailed analysis of relative scour depth at nine OWFs, certain limitations must be addressed to improve the interpretation of the findings. Although the dataset spans multiple years, it represents snapshots in time and may not fully capture the dynamic evolution of scour processes under fluctuating metocean conditions (Matutano et al., 2013; Carpenter et al., 2016). Hindcast data, while valuable for long-term correlations, are often based on limited spatial resolution that may underestimate short-term extreme events such as storm surges
- 782 or localized current variations (Whitehouse et al., 2010; Sturt et al., 2009).
- 783 Using PCA is effective in identifying dominant linear relationships between relative scour depth and key variables;
- 784 however, it may miss critical nonlinear interactions that drive scour processes (Schendel et al., 2020; Lyu et al.,
- 785 2021). While this study incorporates, parameters such as the Keulegan-Carpenter number and the mobility
- 786 parameter, the accuracy of these parameters is are limited by temporal resolution and data availability. -Valuable
- 787 insight was provided into the role of hydrodynamic forcing on sediment mobility through their inclusion; however,
- 788 more detailed and site-specific input data are needed so that their predictive potential can be fully exploited
- 789 (Sheppard et al., 2004; Zhao et al., 2012).
- 790 The next step in this research is to develop data-driven models and investigate the broader implications for regional
- 791 sediment dynamics. Future studies will focus on OWFs located in fine and medium sands where significant scour
- 792 activity is observed. By focusing on these environments, we aim to improve prediction capabilities and better
- 793 understand the mechanisms that drive scour, particularly in areas that are susceptible to substantial sediment
- 794 mobilization.

776

- 795 -Finally, while the present study focused on localized scour processes, the cumulative effects of OWF structures
- 796 on regional sediment transport and marine ecosystems remain a significant knowledge gap (Christiansen et al.,
- 797 2022; Schultze et al., 2021). Future research must employ interdisciplinary methodologies to rigorously assess the
- 798 ecological impacts of sediment mobility and scour on marine habitats. By integrating regional sediment transport
- 799 models with comprehensive ecological assessments, we can optimize offshore wind energy development to meet
- 800 both sustainability and environmental protection goals, ensuring long-term benefits for infrastructure resilience
- 801 and marine ecosystem health.

802 5 Conclusion

Achieving the European Union's (EU) offshore wind energy targets requires development of OWFs in regions with diverse and often poorly understood meteoceanic and geophysical conditions. However, this demand underscores critical knowledge gaps regarding the interaction of these installations with the marine environment, particularly with respect to scour processes and sediment mobilization. A comprehensive understanding of scour dynamics is essential, not only to ensure structural integrity, but also to assess potential impacts on regional sediment transport and broader ecosystem functions.

In this study, high-resolution bathymetry data were used to analyse field-measured relative scour depth of 460 monopiles across nine British OWFs. The analysis included a PCA in which eight hydrodynamic and geotechnical variables were considered to identify the dominant driver influencing relative scour depth variability. This analysis provided a basis for understanding the primary correlations between relative scour depth and metocean site conditions, but also highlighted the complexity of these relationships, requiring further refinement.

The main conclusions can be summarized as follows:

- 849 I 850 e

- (1) Universal drivers of scour: Across all nine OWFs, the PCA the relative water depth-, the relative grain size, the Keulegan-Carpenter number and the mobility parameter as the most influential variables governing scour depth variability. Among these, -the relative water showed the strongest correlation (Fig. 7), where greater relative scour depth occurred in shallower waters, particularly at location with sediments composed of $(63 \le d_{50} < 200 \ \mu m)$ and medium sand $(200 \le d_{50} < -630 \ \mu m)$. In shallow waters the increased kinetic energy promotes stronger down-flow and vortex activity around the pile, enhancing scour, whereas in deeper water, hydrostatic pressure dominates, weakening these effects (Melville, 2008; FHWA, 2012), Furthermore, inclusion of the relative grain size captures the effect of grain-pile scaling, while the Keulegan-Carpenter number and the mobility parameter reflect the influence of flow unsteadiness and sediment mobility thresholds, reinforcing their relevance in realistic scour prediction frameworks.
- (2) **Sediment-specific correlations:** In order to explore the variability within soil classes, the data set was clustered according to d_{50} , and a PCA was applied to each cluster. For fine sand (63 to 200 μ m) and medium sand (200 to 630 μ m), relative water depth was found to be the dominant driver of relative scour depth, demonstrating the sensitivity of these sediment types to hydrodynamic forcing in shallower relative water depth. For coarser sediments, such as coarse sands (630 to 2000 μ m) and fine gravels (2000 to 6300 μ m), the correlations were less pronounced, reflecting a greater resistance to scour. This sediment-specific analysis highlights the importance of considering sediment type when assessing scour susceptibility and designing OWFs, and how different sediment types can influence sediment transport patterns.
- (3) **Site-specific variability:** Due to local factors such as sediment conditions, hydrodynamic conditions, and topography, individual OWFs exhibited unique relative scour depth patterns. For example, London Array (Fig. 12C) showed correlations similar to the global results (Fig. 7), with relative water depth and site topography as the primary influences on scour, followed by current and wave conditions. In contrast, OWFs such as Robin Rigg and Lynn and Inner Dowsing showed no discernible correlations between relative scour depth and the key drivers obtained from the global PCA, highlighting the need for individual analyses to account for local complexities.
- This study also highlights the potential environmental impacts of scour-induced sediment transport. While the primary focus was on identifying the physical drivers of scour, the findings could provide a first step in assessing potential impacts of OWF on the marine environment due to a changed regional sediment mobility. The entrainment of eroded sediment into the water column, with subsequent long-range transport, raises concerns about sediment deposition and potential impacts on benthic habitats and marine wildlife in far-field regions.
- Future research should prioritize the refinement of predictive scour models that incorporate temporal data and expanded hydrodynamic parameters to improve accuracy in diverse sedimentary environments. In addition,

- 851 integrated approaches that combine regional sediment transport modelling with ecological assessments are critical
- 852 for evaluating the cumulative impacts of OWF facilities on marine ecosystems. These efforts will facilitate the
- 853 development of sustainable OWF designs that minimize environmental disturbance while advancing renewable
- 854 energy goals.

- 856 Data availability: The data set used in this study is available in the Marine Data Exchange (MDE)
- 857 (https://www.marinedataexchange.co.uk/) and by the Copernicus Marine Service (CMEMS)
- 858 (https://marine.copernicus.eu/)

859

860

- 861 Authors contribution: K. G.: Writing original draft preparation, visualization, formal analysis,
- 862 conceptualization, methodology. C.J. Writing review & editing, supervision, conceptualization, project
- administration. **G.M.** Writing review & editing, resources. **A.S.** Writing review & editing, methodology. **M.W**.
- 864 Writing review & editing, Supervision. T.S. Writing review & editing, Funding acquisition, Supervision.

865

866 Competing interests: The authors declare that they have no conflict of interest.

867

- 868 Acknowledgements: This work contributes to the DAM Research Mission sustainMare and the project
- 869 CoastalFutures (Project Number: 03F0911G) funded by the German Federal Ministry of Education and Research
- 870 (BMBF). The responsibility for the content of this publication lies with the authors.

871

872

873 References

- 874 Annad, M., Zourgui, N. H., Lefkir, A., Kibboua, A., and Annad, O.: Scour-dependent seismic fragility curves
- 875 considering soil-structure interaction and fuzzy damage clustering: A case study of an Algerian RC Bridge
- with shallow foundations, Ocean Engineering, 275, 114157, 2023.
- 877 Annad, M., Lefkir, A., Mammar-Kouadri, M., and Bettahar, I.: Development of a local scour prediction model
- clustered by soil class, Water Pract. Technol., 16, 1159–1172, 2021.
- 879 Baykal, C., Sumer, B. M., Fuhrman, D. R., Jacobsen, N. G., and Fredsøe, J.: Numerical investigation of flow and
- 880 scour around a vertical circular cylinder, Philos. Trans. R. Soc. A, 373, 20140104,
- https://doi.org/10.1098/rsta.2014.0104, 2015.
- 882 Baelus, L., Bolle, A., and Szengel, V.: Long term scour monitoring around on a sandy seabed, in: Scour and
- Erosion IX: Proceedings of the 9th International Conference on Scour and Erosion (ICSE 2018), November
- 5–8, 2018, Taipei, Taiwan, CRC Press, 2018.
- 885 Baeye, M., and Fettweis, M.: In situ observations of suspended particulate matter plumes at an offshore wind farm,
- 886 southern North Sea, Geo-Mar. Lett., 35, 247–255, 2015.

- 887 Bailey, H., Brookes, K. L., and Thompson, P. M.: Assessing environmental impacts of offshore wind farms:
- lessons learned and recommendations for the future, Aquat. Biosyst., 10, 1–13, https://doi.org/10.1186/2046-
- 889 9063-10-8, 2014.
- 890 Bolle, A., De Winter, J., Goossens, W., Haerens, P., and Dewaele, G.: Scour monitoring around offshore jackets
- and gravity based foundations, in: Proceedings of the Sixth International Conference on Scour and Erosion,
- 892 Paris, France, 27–31, 2012.
- 893 Breusers, H. N. C., Nicollet, G., and Shen, H. W.: Local scour around cylindrical piers, J. Hydraul. Res., 15, 211-
- 894 252, 1977.
- 895 Brignon, J. M., Lejart, M., Nexer, M., Michel, S., Quentric, A., Thiebaud, L.: A risk-based method to prioritize
- cumulative impacts assessment on marine biodiversity and research policy for offshore wind farms in France,
- 897 Environ. Sci. Pol., 128, 264–276, https://doi.org/10.1016/j.envsci.2021.12.003, 2022.
- 898 Carpenter, J. R., Merckelbach, L., Callies, U., Clark, S., Gaslikova, L., and Baschek, B.: Potential impacts of
- 899 offshore wind farms on North Sea stratification, PLOS ONE, 11,
- 900 https://doi.org/10.1371/journal.pone.0159512, 2016.
- 901 Carreiras, J., Larroudé, P., Seabra-Santos, F., and Mory, M.: Wave scour around piles, in: Coastal Engineering
- 902 2000, 1860–1870, 2001.
- 903 Chen, H., Zhang, J., Guo, Y., Cui, L., Guan, D., and Jiang, L.: Laboratory modelling study on the scour
- characteristics around a jacket foundation subjected to combined wave-current loading, Renew. Energy,
- 905 122443, 2025.
- 906 Chiew, Y. M.: Local scour at bridge piers, Publication of: Auckland University, New Zealand, 1984.
- 907 Christiansen, N., Daewel, U., Djath, B., and Schrum, C.: Emergence of large-scale hydrodynamic structures due
- to atmospheric offshore wind farm wakes, Front. Mar. Sci., 64, https://doi.org/10.3389/fmars.2022.818501,
- 909 2022.
- 910 CMEMS: Atlantic European North West Shelf Ocean Physics Reanalysis, https://doi.org/10.48670/moi-00059
- 911 and 10.48670/moi-00060, 2023.
- 912 Corvaro, S., Mancinelli, A., and Brocchini, M.: Flow dynamics of waves propagating over different permeable
- 913 beds, Coastal Engineering Proceedings, 35, 35–35, 2016.
- 914 COWRIE: A Further Review of Sediment Monitoring Data, Cowrie Ltd., Project reference ScourSed-09, 2010.
- 915 DECC: Dynamics of scour pits and scour protection Synthesis report and recommendations (Milestones 2 and
- 3), Department for Energy and Climate Change, Final Report, 2008.
- 917 Du, S., Wu, G., Zhu, D. Z., Wang, R., Lu, Y., and Liang, B.: Experimental study of local scour around submerged
- 918 square piles in combined waves and current, Ocean Eng., 266, 113176, 2022.
- 919 Escarameia, M., and May, R. W. P.: Scour around structures in tidal flows, HR Wallingford, Wallingford, U.K.,
- 920 1999.
- 921 EGS (International) Ltd.: Lynn and Inner Dowsing Offshore Wind Farms, Year 3 Post-Construction Survey
- 922 (2011), Phase 1 Geophysical Survey, Job No. 4918, Final Report Rev 7, CREL Reference No LD-O-EV-
- 923 013-0000-000000-368-D, Marine Data Exchange, https://www.marinedataexchange.co.uk/details/TCE-
- 924 1041/2011-egs-lynn-and-inner-dowsing-year-3-post-construction-survey-phase-1---geophysical-
- 925 survey/summary, 2012.
- 926 EGS (International) Ltd.: Lynn and Inner Dowsing Offshore Wind Farms (October 2012), Job No. 5038, Final
- Page 10. Report Rev1, Marine Data Exchange, https://www.marinedataexchange.co.uk/details/TCE-1076/2012-egs-

- 928 lynn-and-inner-dowsing-offshore-wind-farms-post-construction-hydrographic-and-geophysical-
- 929 survey/summary, 2013.
- 930 EU: An EU Strategy to harness the potential of offshore renewable energy for a climate-neutral future, European
- 931 Commission, Communication COM/2020/741 final, 2020.
- 932 Federal Highway Administration (FHWA): Evaluating scour at bridges (HEC-18, Publication No. FHWA-HIF-
- 933 12-003), U.S. Department of Transportation, 2012.
- 934 Gabriel, K. R.: The Biplot Graphic Display of Matrices with Application to Principal Component Analysis,
- 935 Biometrika, 58, 453–467, https://doi.org/10.1093/biomet/58.3.453, 1971.
- 936 Gazi, A. H., Purkayastha, S., and Afzal, M. S.: The equilibrium scour depth around a pier under the action of
- collinear waves and current, J. Mar. Sci. Eng., 8, 36, 2020.
- 938 Guşatu, L. F., Menegon, S., Depellegrin, D., Zuidema, C., Faaij, A., and Yamu, C.: Spatial and temporal analysis
- of cumulative environmental effects of offshore wind farms in the North Sea basin, Sci. Rep., 11, 1–18,
- 940 https://doi.org/10.1038/s41598-021-89537-1, 2021.
- 941 Harasti, A., Gilja, G., Adžaga, N., and Škreb, K. A.: Principal Component Analysis in development of empirical
- 942 scour formulae, in: Proceedings of the 7th IAHR Europe Congress, Athens, Greece, 7–9 September 2022,
- 943 271–272, 2022.
- 944 Harris, J. M., Herman, W. M., and Cooper, B. S.: Offshore windfarms: an approach to scour assessment, in: Y. M.
- 945 Chiew, S.-Y. Lim, and N.-S. Cheng (Eds.), Proceedings of the 2nd International Conference on Scour and
- 946 Erosion, Stallion Press, Singapore, 283–291, 2004.
- 947 Harris, J. M., Tavouktsoglou, N. S., Couldrey, A., Whitehouse, R. J., and Klapper, J.: Scour prediction in cohesive
- 948 marine soils: a hybrid approach, ISSMGE Int. J. Geoeng. Case Histories, 7, 59–75, 2023.
- 949 Harris, J., and Whitehouse, R. J. S.: Scour prediction in non-uniform soils: Undrained shear strength and
- 950 erodibility, 2014.
- 951 Hancu, S.: Sur le calcul des affouillements locaux dans la zone des piles de ponts, in: Proceedings of the 14th
- 952 IAHR Congress, 299–313, 1971.
- 953 Hu, R., Wang, X., Liu, H., and Lu, Y.: Experimental study of local scour around tripod foundation in combined
- ollinear waves-current conditions, Journal of Marine Science and Engineering, 9(12), 1373, 2021.
- 955 Jolliffe, I. T., and Cadima, J.: Principal component analysis: a review and recent developments, Philosophical
- 956 Transactions of the Royal Society A: Mathematical, Physical and Engineering Sciences, 374(2065),
- 957 20150202, 2016.
- 958 Kenyon, N., and Cooper, B.: Sand banks, sand transport and offshore wind farms, Gov. British, 2005.
- 959 Laursen, E. M.: An analysis of relief bridge scour, J. Hydraul. Div., Proc. ASCE, 89(HY3), 93–118, 1963.
- Link, O., and Zanke, U.: On the time-dependent scour-hole volume evolution at a circular pier in uniform coarse sand, in: Proc. 2nd International Conference on Scour and Erosion (ICSE), 2004.
- 962 Lloret, J., Turiel, A., Solé, J., Berdalet, E., Sabatés, A., Olivares, A., Gili, J.-M., Vila-Subirós, J., and Sardá, R.:
- Unravelling the ecological impacts of large-scale offshore wind farms in the Mediterranean Sea, Sci. Total
- 964 Environ., 824, 153803, 2022.
- 965 Louwersheimer, W. F., Verhagen, H. J., and Olthof, J.: Scour around an offshore wind turbine, in: Coastal
- 966 Structures 2007 Proceedings of the 5th Coastal Structures International Conference, CST07, Venice, Italy,
- 967 1903–1912, 2009.
- 968 London Array Ltd.: Environmental Statement Volume 1: Offshore Works, Technical report, London Array Ltd.,
- 969 2005.

- 970 Lyu, X., Cheng, Y., Wang, W., An, H., and Li, Y.: Experimental study on local scour around submerged monopile
- under combined waves and current, Ocean Eng., 240, 109929, 2021.
- 972 May, R. P., and Willoughby, I. R.: Local scour around large obstructions, HR Wallingford Report SR240, 1990.
- 973 Matutano, C., Negro, V., López-Gutiérrez, J.-S., and Esteban, M. D.: Scour prediction and scour protections in
- 974 offshore wind farms, Renew. Energy, 57, 358–365, 2013.
- 975 Matthieu J., Raaijmakers T. Interaction between Offshore Pipelines and Migrating Sand Waves. 2012.
- 976 McGovern, D. J., Ilic, S., Folkard, A. M., McLelland, S. J., and Murphy, B. J.: Time development of scour around
- a cylinder in simulated tidal currents, J. Hydraul. Eng., 140(6), 04014014, 2014.
- 978 Melling, G. J.: Hydrodynamic and geotechnical controls of scour around offshore monopiles, University of
- 979 Southampton, Ocean and Earth Science, Doctoral Thesis, 250 pp., 2015.
- 980 Melville, B.: The physics of local scour at bridge piers, in: Proceedings of the 4th International Conference on
- 981 Scour and Erosion, 28–38, 2008.

- 982 Noormets, R., Ernstsen, V., Bartholoma, A., Flemming, B., and Hebbeln, D.: Local scour in a tidal environment:
- a case study from the Otzumer Balje tidal inlet, southern North Sea, Poster reproduced in Appendix A of
- 984 Offshore Center Danmark, 2006, 2003.
- 985 Qi, W. G., and Gao, F. P.: Physical modeling of local scour development around a large-diameter monopile in
- combined waves and current, Coast. Eng., 83, 72–81, 2014.
- 987 Qi, M., Li, J., and Chen, Q.: Comparison of existing equations for local scour at bridge piers: parameter influence
- 988 and validation, Nat. Hazards, 82, 2089–2105, 2016.
- 989 Qu, L., An, H., Draper, S., Watson, P., Zhao, M., Harris, J., Whitehouse, R., and Zhang, D.: A review of scour
- impacting monopiles for offshore wind, Ocean Engineering, 301, 117385, 2024.
- 992 Richardson, M. D., Valent, P., Briggs, K., Bradley, J., and Griffin, S.: NRL mine burial experiments, in:
- 993 Proceedings of the 2nd Australian-American Joint Conference on the Technologies of Mines and Mine
- 994 Countermeasures, Sydney, Australia, 1–23, 2001.
- 995 Rivier, A., Bennis, A. C., Pinon, G., Magar, V., and Gross, M.: Parameterization of wind turbine impacts on
- hydrodynamics and sediment transport, Ocean Dyn., 66, 1285–1299, 2016.
- 997 Roulund, A., Sutherland, J., Todd, D., and Sterner, J.: Parametric equations for Shields parameter and wave orbital
- 998 velocity in combined current and irregular waves, 2016
- 999 Rudolph, D., Bos, K. J., Luijendijk, A. P., Rietema, K., and Out, J. M. M.: Scour around offshore structures –
- Analysis of field measurements, in: Y. M. Chiew, S.-Y. Lim, and N.-S. Cheng (Eds.), Proceedings of the 2nd
- 1001 International Conference on Scour and Erosion, Stallion Press, Singapore, 400–407, 2004.
- 1002 Saathoff, J. E., Goldau, N., Achmus, M., Schendel, A., Welzel, M., and Schlurmann, T.: Influence of scour and
- scour protection on the stiffness of monopile foundations in sand, Appl. Ocean Res., 144, 103920, 2024.
- 1004 Sarkar, A.: Scour and flow around submerged structures, in: Proceedings of the Institution of Civil Engineers-
- Water Management, 167(2), 65–78, Thomas Telford Ltd., February 2014.
- 1006 Sarmiento, J., Guanche, R., Losada, I. J., Rosendo, E. M., Guindo, A., and de Guevara, J. L.: Scour processes
- around pile clusters of jacket foundations under steady currents, Ocean Eng., 313, 119502, 2024.
- 1008 Schendel, A.: Wave-current-induced scouring processes and protection by widely graded material, Leibniz
- University Hannover, Dissertation, https://doi.org/10.15488/4453, 2018.

- 1010 Schendel, A., Welzel, M., Schlurmann, T., and Hsu, T.-W.: Scour around a monopile induced by directionally
- spread irregular waves in combination with oblique currents, Coast. Eng., 161, 103751,
- 1012 https://doi.org/10.1016/j.coastaleng.2020.103751, 2020.
- 1013 Schultze, L. K. P., Merckelbach, L. M., Horstmann, J., Raasch, S., and Carpenter, J. R.: Increased mixing and
- turbulence in the wake of offshore wind farm foundations, J. Geophys. Res. Oceans, 125(8), e2019JC015858,
- **1015** 2020.
- 1016 Sheppard, D. M., Odeh, M., and Glasser, T.: Large scale clear-water local pier scour experiments, J. Hydraul.
- 1017 Eng., 130(10), 957–963, 2004.
- 1018 Shields, M. A., Woolf, D. K., Grist, E. P., Kerr, S. A., Jackson, A. C., Harris, R. E., and Side, J.: Marine renewable
- energy: The ecological implications of altering the hydrodynamics of the marine environment, Ocean Coast.
- 1020 Manag., 54(1), 2–9, 2011.
- 1021 Sheppard, D. M., Zhao, G., and Ontowirjo, B.: Local scour near single piles in steady currents, in: Water Resources
- 1022 Engineering, pp. 1809–1813, ASCE, 1995.
- 1024 Sheppard, D. M., Ontowirjo, B., and Zhao, G.: Conditions of Maximum Local Scour, in: Proceedings of Stream
- Stability and Scour at Highway Bridges, Resources Engineering Conference 1991–1998, edited by
- Richardson, E. V., and Lagasse, P. F., ASCE, Reston, VA, 1999.
- 1027

- 1028 Smith, J. D., and McLean, S. R.: Spatially averaged flow over a wavy surface, J. Geophys. Res., 82(12), 1735-
- **1029** 1746, 1977.
- 1030 Soulsby, R. L., and Whitehouse, R. J. S.: Threshold of sediment motion in coastal environments, in: Pacific Coasts
- and Ports '97: Proceedings of the 13th Australasian Coastal and Ocean Engineering Conference and the 6th
- Australasian Port and Harbour Conference, Vol. 1, pp. 145–150, Centre for Advanced Engineering, University
- of Canterbury, Christchurch, NZ, 1997.
- 1034 Soulsby, R.: Dynamics of Marine Sands, Thomas Telford Ltd., 1997.
- 1035 Stahlmann, A.: Numerical and experimental modeling of scour at foundation structures for offshore wind turbines,
- in: ISOPE International Ocean and Polar, June 2013.
- 1037 Sturt, F., Dix, J. K., and EMU Ltd.: The Outer Thames Estuary Regional Environmental Characterisation, Marine
- Aggregate Levy Sustainability Fund, 09/J/1/06/1305/0870, Technical report, Marine Aggregate Levy
- 1039 Sustainability Fund, 2009.
- 1040 Sumer, B. M., Fredsøe, J., and Christiansen, N.: Scour around vertical pile in waves, J. Waterway Port Coastal
- 1041 Ocean Eng., 118, 15, 1992.
- 1042 Sumer, B. M., and Fredsøe, J.: Scour around pile in combined waves and current, J. Hydraul. Eng., 127(5), 403-
- **1043** 411, 2001.
- 1044 Sumer, B. M., Petersen, T. U., Locatelli, L., Fredsøe, J., Musumeci, R. E., and Foti, E.: Backfilling of a scour hole
- around a pile in waves and current, J. Waterway, Port, Coastal, Ocean Eng., 139(1), 9–23, 2013.
- 1046 Teilmann, J., and Carstensen, J.: Negative long term effects on harbour porpoises from a large scale offshore wind
- farm in the Baltic evidence of slow recovery, Environ. Res. Lett., 7, https://doi.org/10.1088/1748-
- 1048 9326/7/4/045101, 2012.
- 1049 Van Rijn, L. C.: Sediment transport, part I: bed load transport, J. Hydraul. Eng., 110(10), 1431–1456, 1984.
- 1050 Vanhellemont, Q., and Ruddick, K.: Turbid wakes associated with offshore wind turbines observed with Landsat
- 1051 8, Remote Sens. Environ., 145, 105–115, 2014.
- 1052 Walker, W.: Field measurements of local pier scour in a tidal inlet, MSc, University of Florida, 1995.

- 1053 Watson, S. C., Somerfield, P. J., Lemasson, A. J., Knights, A. M., Edwards-Jones, A., Nunes, J., and Beaumont,
- N. J.: The global impact of offshore wind farms on ecosystem services, Ocean Coast. Manag., 249, 107023,
- 1055 https://doi.org/10.1016/j.ocecoaman.2024.107023, 2024.
- 1056 Welzel, M., Schendel, A., Schlurmann, T., and Hildebrandt, A.: Volume-based assessment of erosion patterns
- around a hydrodynamic transparent offshore structure, Energies, 12(16), 3089, 2019.
- 1058 Welzel, M.: Wave-current-induced scouring processes around complex offshore structures, 2021.
- 1059 Welzel, M., Schendel, A., Satari, R., Neuweiler, I., and Schlurmann, T.: Spatio-temporal analysis of scour around
- complex offshore foundations under clear water and live bed conditions, Ocean Eng., 298, 117042, 2024.
- 1061 Wilson, J. C., and Elliott, M.: The habitat-creation potential of offshore wind farms, Wind Energy, 12(2), 203-
- 1062 212, 2009.
- 1063 Whitehouse, R.: Dynamics of estuarine muds. Thomas Telford, 2000.
- Whitehouse, R. J. S., Harris, J. M., Mundon, T. R., and Sutherland, J.: Scour at offshore structures, in: Proceedings
- of the 5th International Conference on Scour and Erosion, San Francisco, 11–20, 2010.
- 1066 Whitehouse, R. J. S., Harris, J. M., Sutherland, J., and Rees, J.: The nature of scour development and scour
- protection at onshore wind farm foundations, Mar. Pollut. Bull., 62(1), 73–88, 2011.
- 1068 Whitehouse, R. J. S., and Harris, J.: Scour prediction offshore and soil erosion testing, HR Wallingford Report,
- 1069 2014.

- 1070 Yao, Y., Chen, Y., Zhou, H., and Yang, H.: Numerical modeling of current loads on a net cage considering fluid-
- 1071 structure interaction, J. Fluids Struct., 62, 350–366, 2016.
- 1072 Zhao, M., Zhu, X., Cheng, L., and Teng, B.: Experimental study of local scour around subsea caissons in steady
- 1073 currents, Coast. Eng., 60, 30–40, 2012.
- 1074 Zanke, U. C. E., Hsu, T.-W., Roland, A., Link, O., and Diab, R.: Equilibrium scour depths around piles in
- noncohesive sediments under currents and waves, Coastal Eng., 58(10), 986–991, 2011.